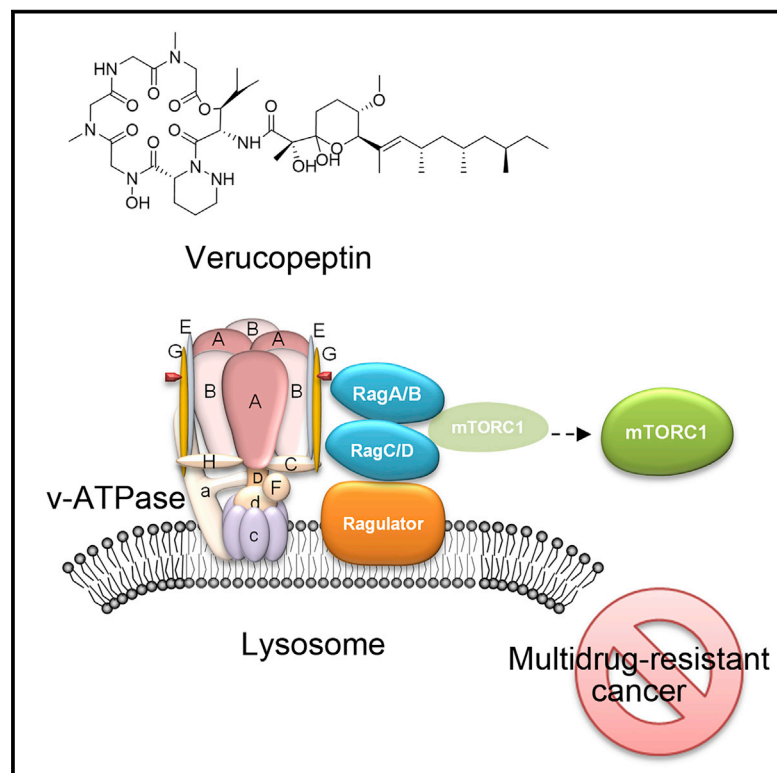


# Cell Chemical Biology

## Pharmacological Targeting of Vacuolar H<sup>+</sup>-ATPase via Subunit V1G Combats Multidrug-Resistant Cancer

### Graphical Abstract



### Authors

Yuezhou Wang, Lei Zhang, Yanling Wei, ..., Melissa S. Jurica, Cyril H. Benes, Xianming Deng

### Correspondence

xmdeng@xmu.edu.cn

### In Brief

Alternative strategy for treating multidrug-resistant (MDR) cancer is needed. Wang et al. show that the natural product verucopeptin kills MDR cancer by targeting the ATP6V1G subunit of v-ATPase, which leads to strong inhibition of both v-ATPase activity and mTORC1 signaling.

### Highlights

- The natural product verucopeptin exhibits antitumor activity against MDR cancers
- Verucopeptin directly targets the v-ATPase ATP6V1G subunit
- Verucopeptin kills MDR cancer cells by inhibition of both v-ATPase and mTORC1
- Verucopeptin suppresses MDR cancer progression *in vivo*

Article

# Pharmacological Targeting of Vacuolar H<sup>+</sup>-ATPase via Subunit V1G Combats Multidrug-Resistant Cancer

Yuezhou Wang,<sup>1,2,12</sup> Lei Zhang,<sup>1,2,12</sup> Yanling Wei,<sup>1,2,12</sup> Wei Huang,<sup>1,2,12</sup> Li Li,<sup>1,2,12</sup> An-an Wu,<sup>3,4</sup> Anahita Dastur,<sup>5</sup> Patricia Greninger,<sup>5</sup> Walter M. Bray,<sup>6</sup> Chen-Song Zhang,<sup>1,2</sup> Mengqi Li,<sup>1,2</sup> Wenhua Lian,<sup>1,2</sup> Zhiyu Hu,<sup>1,2</sup> Xiaoyong Wang,<sup>7</sup> Gang Liu,<sup>7</sup> Luming Yao,<sup>1,2</sup> Jih-Hwa Guh,<sup>8</sup> Lanfen Chen,<sup>1,2</sup> Hong-Rui Wang,<sup>1,2</sup> Dawang Zhou,<sup>1,2</sup> Sheng-Cai Lin,<sup>1,2</sup> Qingyan Xu,<sup>1,2</sup> Yuemao Shen,<sup>9</sup> Jianming Zhang,<sup>10</sup> Melissa S. Jurica,<sup>11</sup> Cyril H. Benes,<sup>5</sup> and Xianming Deng<sup>1,2,13,\*</sup>

<sup>1</sup>State Key Laboratory of Cellular Stress Biology, Innovation Center for Cell Signaling Network, School of Life Sciences, Xiamen University, Xiamen, Fujian 361102, China

<sup>2</sup>State-province Joint Engineering Laboratory of Targeted Drugs from Natural Products, Xiamen University, Xiamen, Fujian 361102, China

<sup>3</sup>State Key Laboratory for Physical Chemistry of Solid Surface, College of Chemistry and Chemical Engineering, Xiamen University, Xiamen, Fujian 361005, China

<sup>4</sup>Fujian Provincial Key Laboratory of Theoretical and Computational Chemistry, Xiamen, Fujian, China

<sup>5</sup>Massachusetts General Hospital Cancer Center, Harvard Medical School, Charlestown, MA 02129, USA

<sup>6</sup>Department of Chemistry and Biochemistry, University of California, Santa Cruz, CA 95064, USA

<sup>7</sup>State Key Laboratory of Molecular Vaccinology and Molecular Diagnostics Center for Molecular Imaging and Translational Medicine, School of Public Health, Xiamen University, Xiamen 361102, China

<sup>8</sup>School of Pharmacy, National Taiwan University, Taipei, Taiwan

<sup>9</sup>School of Pharmaceutical Sciences, Shandong University, Jinan, Shandong 250012, China

<sup>10</sup>National Translational Research Center Ruijin Hospital, Shanghai Jiaotong University School of Medicine, Shanghai 200025 China

<sup>11</sup>Department of Molecular Cell and Developmental Biology and Center for Molecular Biology of RNA, University of California, Santa Cruz, CA 95064, USA

<sup>12</sup>These authors contributed equally

<sup>13</sup>Lead Contact

\*Correspondence: [xmdeng@xmu.edu.cn](mailto:xmdeng@xmu.edu.cn)

<https://doi.org/10.1016/j.chembiol.2020.06.011>

## SUMMARY

Multidrug resistance (MDR) in cancer remains a major challenge for the success of chemotherapy. Natural products have been a rich source for the discovery of drugs against MDR cancers. Here, we applied high-throughput cytotoxicity screening of an in-house natural product library against MDR SGC7901/VCR cells and identified that the cyclodepsipeptide veruceptin demonstrated notable antitumor potency. Cytological profiling combined with click chemistry-based proteomics revealed that ATP6V1G directly interacted with veruceptin. ATP6V1G, a subunit of the vacuolar H<sup>+</sup>-ATPase (v-ATPase) that has not been previously targeted, was essential for SGC7901/VCR cell growth. Veruceptin exhibited strong inhibition of both v-ATPase activity and mTORC1 signaling, leading to substantial pharmacological efficacy against SGC7901/VCR cell proliferation and tumor growth *in vivo*. Our results demonstrate that targeting v-ATPase via its V1G subunit constitutes a unique approach for modulating v-ATPase and mTORC1 signaling with great potential for the development of therapeutics against MDR cancers.

## INTRODUCTION

Drug resistance causes treatment failure in nearly 90% of patients with metastatic cancer (Holoan et al., 2013; Longley and Johnston, 2005; Sharma et al., 2018). Multidrug resistance (MDR), which develops when cancer cells become resistant to multiple antineoplastic drugs with different structures and mechanisms during the course of chemotherapeutic treatment, is the major barrier for successful therapeutic interventions in cancer (Gillet and Gottesman, 2010; Montazami et al., 2015; Szakacs et al., 2006). Overcoming MDR has been a high priority for both clinical oncologists and anticancer drug hunters. Numerous

mechanisms have been reported to be involved in the development of MDR to chemotherapy, such as increased drug efflux, decreased drug uptake, and accelerated drug metabolism. Overexpression of ATP-binding cassette (ABC) transporters, which pump drugs out of cells through the cell membrane, has long been considered a common mechanism of MDR (Rees et al., 2009). Unfortunately, the clinical performance of ABC transporter-targeted inhibitors seems unsatisfactory (Robey et al., 2018). Therefore, alternative strategies and new chemical entities for combating MDR cancers are urgently needed.

As a result of interaction and evolutionary optimization by their biosynthetic enzymes, natural products have long been

considered valuable sources for drug development (Newman and Cragg, 2016; Silver, 2015). Unlike synthetic small molecules, natural products occupy unique chemical environments by bearing complicated 3D architectures and multiple stereocenters (Over et al., 2013). A few recent studies have reported applications of natural products in treating MDR cancers. For example, tetrandrine, a bisbenzylisoquinoline alkaloid identified in the Chinese medicinal herb *Radix Stephanae tetrandrae*, reverses MDR in MCF-7/adr cells both *in vitro* and in xenograft models (Kumar and Jaitak, 2019). Rhamnetin, derived from Persian berries, sensitizes hepatocellular HepG2/ADR cells to sorafenib via the Notch receptor 1 (Notch1) pathway (Jia et al., 2016). Thus, natural products hold great promise for identifying new mechanisms and chemical entities to combat MDR.

The vacuolar H<sup>+</sup>-ATPase (v-ATPase) is an ATP-dependent H<sup>+</sup> transporter that pumps protons across intracellular and plasma membranes through a highly coordinated, multisubunit protein complex. The “catalytic hexamer” A<sub>3</sub>B<sub>3</sub> in the V1 sector catalyzes ATP-driven rotation of the central rotors D and F, which in turn, via the V0d bridge, rotate the c ring that is embedded in the lipid bilayer for proton transport (Oot et al., 2017; Roh et al., 2018; Zhao et al., 2015). The three peripheral stalks (the EG1-3 heterodimer) connect the V0 and V1 sectors via subunits C, H, and a (Arai et al., 2013; Nakanishi et al., 2018). The v-ATPase plays a critical role in pH homeostasis, nutrient sensing (Zhang et al., 2014, 2016), autophagy (Chung et al., 2019), and xenophagy (Xu et al., 2019) in normal cells and, to a much greater extent, in tumor cells (Bonam et al., 2019; Stransky et al., 2016). Disrupted or impaired lysosomal activity and v-ATPase function activate critical cellular pathways, such as mechanistic target of rapamycin kinase complex 1 (mTORC1) signaling (Zoncu et al., 2011), thus helping to establish and maintain the acidic environment for malignant cell progression, remote spread, and chemoresistance (Webb et al., 2011). Overexpression or activation of the v-ATPase on the lysosomal surface and tumor cell plasma membrane of tumor cells can acidify the extracellular environment and lysosomal lumen. Many drugs, especially weak bases, are protonated at low pH and thus lose the ability to cross the cellular plasma membrane or become trapped in acidic vesicles, a phenomenon that partially accounts for drug resistance (Simon et al., 1994; Stransky et al., 2016; Vukovic and Tannock, 1997). Therefore, pharmacological targeting of the v-ATPase may be a promising approach for the development of antitumor therapies, especially therapies for MDR cancers.

Here, we identified the cyclodepsipeptide verucopeptin (VE) from an in-house natural product library (~2,000 compounds) with nanomolar to low micromolar activity against MDR SGC7901/VCR and K562R cells. Through a combination of image-based cytological profiling and chemical proteomics, we provide what we believe is the first evidence that VE is an inhibitor of the peripheral stalk of the v-ATPase. The interaction between VE and the ATP6V1G subunit leads to substantial inhibition of v-ATPase activity and downstream mTORC1 signaling, thereby contributing to its excellent pharmacological efficacy against MDR cancer cells *in vitro* as well as in xenograft models *in vivo*. These data demonstrate that VE can be used as a pharmacological probe to investigate v-ATPase and mTORC1 biology and indicate its therapeutic role in MDR cancers.

## RESULTS

### Identification of VE as a Promising Agent against MDR Cancer Cells

In an effort to identify new pharmacological modalities effective against MDR cancer cells, we performed a cellular-based cytotoxicity screen using SGC7901/VCR cells, a vincristine-induced MDR gastric cancer cell line. SGC7901/VCR cells show broad resistance to clinical chemotherapeutic drugs, such as Taxol and cisplatin as well as to cytotoxic agents, such as the HSP90 inhibitor geldanamycin and proteasome inhibitor MG132 (Figure 1A). After screening an in-house library of natural products derived from microorganisms, VE (Figure 1B), a compound isolated from the mangrove rhizosphere bacterium *Actinomyces* sp. XM-4-3 was identified to exhibit notable potency against MDR cells, with a half-maximal inhibitory concentration (IC<sub>50</sub>) value of 1.4 μM (Figure 1A). We then tested another MDR chronic myelogenous leukemia cell line, K562R. K562R cells were reported to be induced by doxorubicin and exhibit an MDR phenotype with increased expression of ABC transporters (Ning et al., 2018). As expected, VE also showed excellent antitumor activity against K562R cells, with an IC<sub>50</sub> of 388 nM, although these cells exhibit resistance to clinical chemotherapeutic drugs, such as Taxol and vincristine at concentrations of 10 μM (Figure 1C). These data demonstrate the excellent potential activity of VE against multiple MDR cancer cells.

VE, which belongs to the family of piperazine acid-containing pyranolated cyclodepsipeptides (PA-PCDs) (Hale et al., 2010; Oelke et al., 2011), was isolated for the first time in 1993 from *Actinomyces verrucosospora* Q886-2 and reported to exhibit significant therapeutic activity with prolongation of the lifespan in mice transplanted with B16 melanoma cells (Nishiyama et al., 1993; Sugawara et al., 1993). However, the precise mechanism of action of VE remains elusive. Substructure searches revealed several previously identified PA-PCDs with exceptional antibiotic abilities (Figure S1). Among these compounds, azinotricin is documented as the most potent Gram-positive antibiotic ever discovered, displaying minimum inhibitory concentration values ranging from 0.001 to 0.016 μg/mL against 51 different bacterial strains (Maehr et al., 1986). Similarly, GE3 exerts a substantial effect on tumor regression in a mouse xenograft model of the currently incurable PSN1 human pancreatic carcinoma (Sakai et al., 1997). Together, the fascinating structure of VE and its impressive bioactivity against MDR cells prompted us to investigate its biological application and mechanism of action.

### VE Is a Potent Antitumor Agent Both *In Vitro* and *In Vivo*

To better understand the potential pharmacological efficacy of VE against human cancers, we profiled VE across a large panel of 1,094 cancer cell lines from the Center for Molecular Therapeutics (Massachusetts General Hospital Cancer Center, Harvard Medical School) (Table S1) (Garnett et al., 2012). VE showed broad antiproliferative activity, with IC<sub>50</sub> values of less than 100 nM against 66% of the cell lines evaluated (Figure 1D). Moreover, VE exhibited tissue specificity; a larger proportion of cell lines of specific cancer types, such as leukemia, lymphoma, and melanoma, were classified in the lower IC<sub>50</sub> groups, while the higher IC<sub>50</sub> groups comprised cell lines of other cancer types, such as non-small cell lung cancer. More importantly, mice treated with VE at a low dosage of 1 mg kg<sup>-1</sup> twice daily showed significant regression

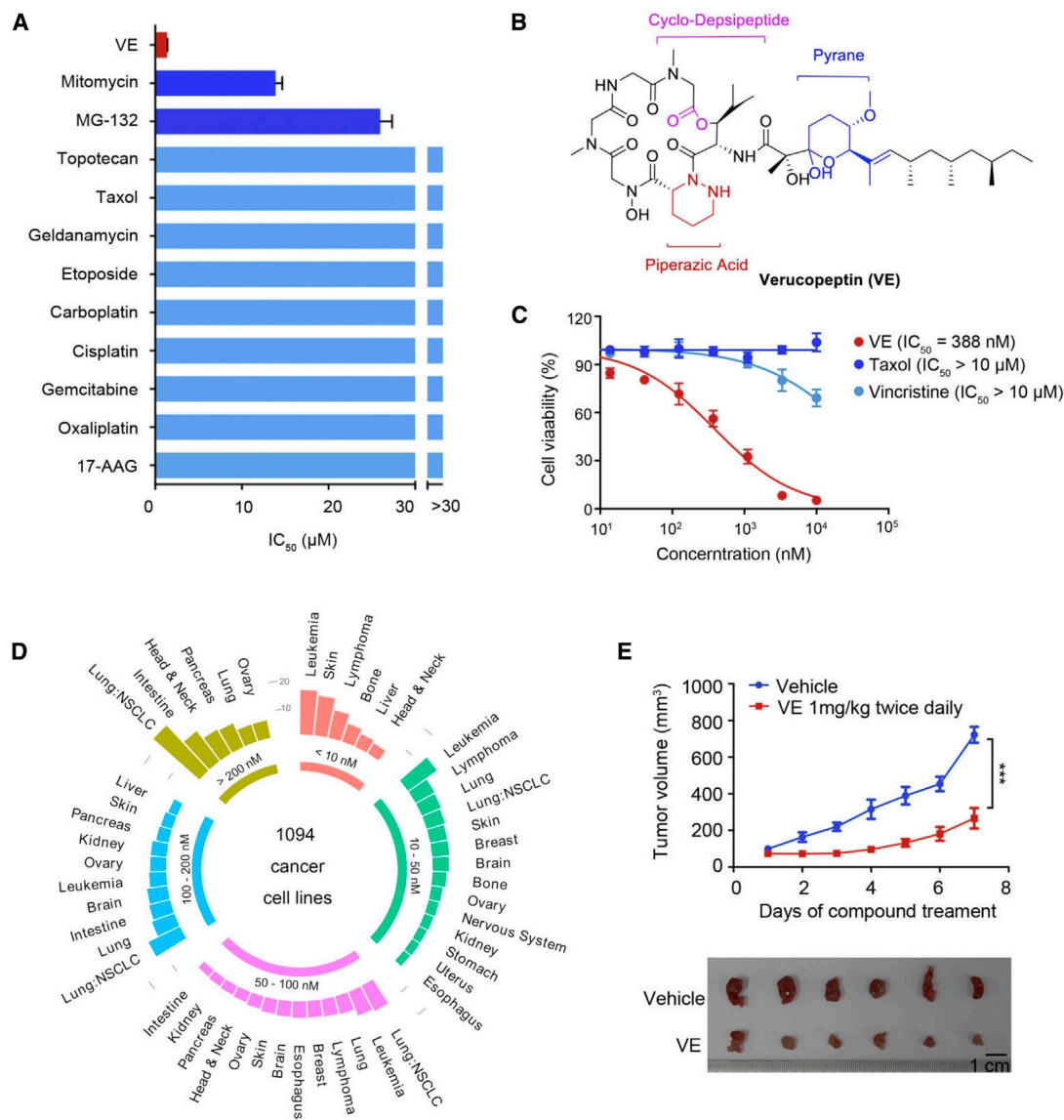


**Figure 1. VE Is a Promising Antitumor Agent *In Vitro* and *In Vivo***

(A) IC<sub>50</sub> values of indicated compounds against MDR gastric cancer cell SGC7901/VCR tested by MTS assay. If cell viability was higher than 50% upon the maximum concentration (30 μM) used in this assay, IC<sub>50</sub> value was denoted as >30 μM.

(B) Chemical structure of VE.

(C) IC<sub>50</sub> values of indicated compounds against MDR chronic myelogenous leukemia cell K562R tested by MTS assay.

(D) A total of 1,094 cancer cell lines from a range of cancer types was examined for anti-proliferative activity by VE. Overview of IC<sub>50</sub> values is shown. The bars represent the proportion of each type of cancer in the indicated subgroups categorized by IC<sub>50</sub> values.

(E) Tumor volume of A375 xenograft model. Data are represented as mean ± SEM, n = 6, p value by Student's t test. \*\*\*p < 0.001.

See also Figure S1 and Table S1.

of tumor growth in a xenograft mouse model established with human melanoma A375 cells (Figure 1E). Cumulatively, these findings indicate that VE exhibits potent *in vitro* and *in vivo* antitumor activity against both primary and MDR cancer cells, highlighting its substantial potential for therapeutic application.

### VE Interferes with Lysosomes

To investigate the molecular mechanism underlying the cytotoxicity of VE, we used a cytological profiling assay to compare the

cellular effects of VE with those of a panel of 480 compounds with known bioactivity (Schulze et al., 2013). The assay used a high-content, image-based screening technology to monitor changes in over 200 features of HeLa cells related to the cytoskeleton, nuclear size and morphology, DNA replication, and cell mitosis and proliferation upon exposure to a compound. Cluster analysis was used to group compounds that generated similar phenotypic responses. The cytological profiling data showed that VE triggered cellular changes in a dose-dependent

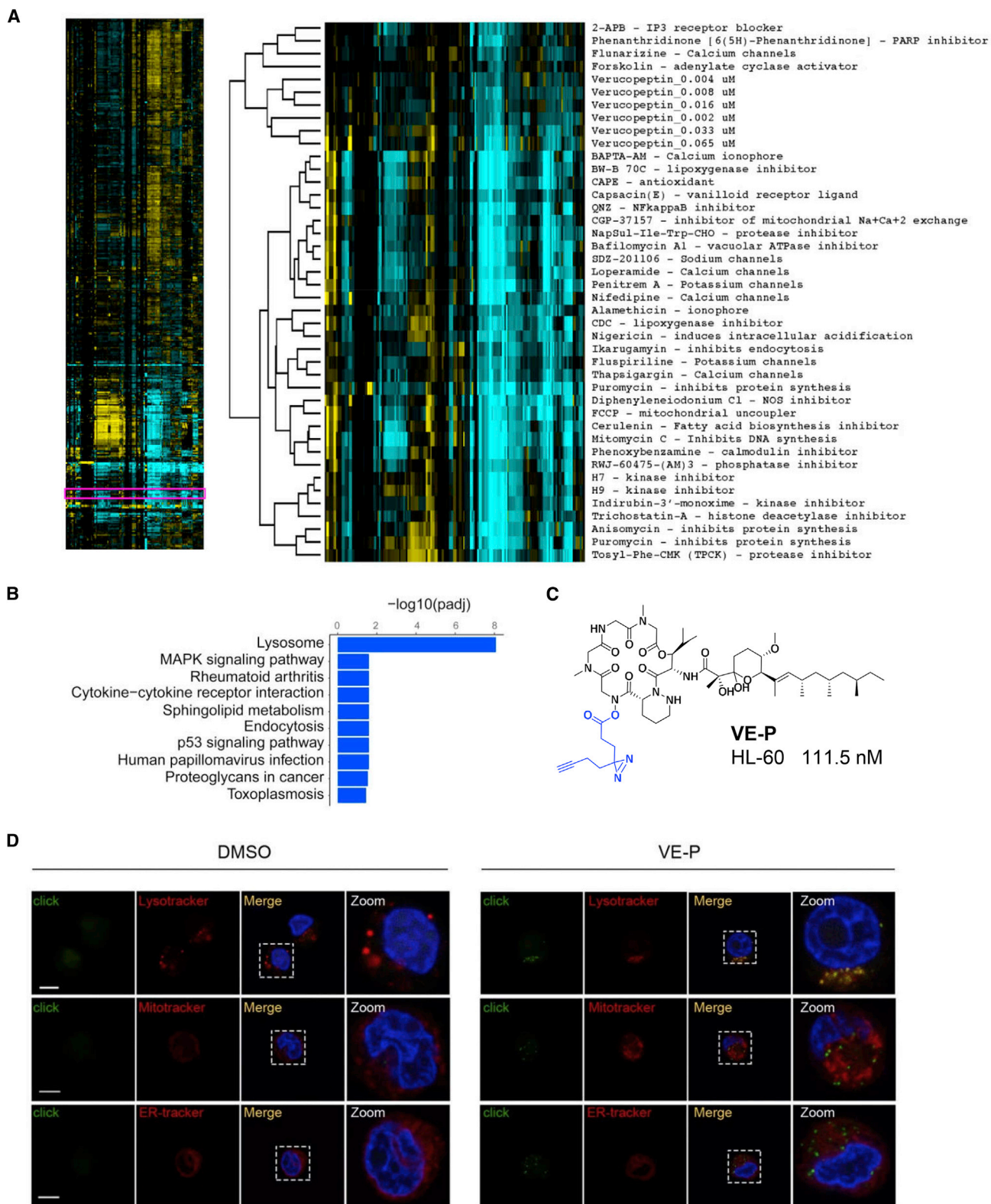


**Figure 2. VE Physically Accumulates in Lysosomes**

(A) The cytological profile for VE. The left panel shows a cluster analysis of the effects of VE and 480 other compounds with known biological activity on HeLa cells. Each row represents a different drug treatment while columns indicate the change in different cell parameters relative to the DMSO control. (Color intensity

(legend continued on next page)

manner. Treatment with 2–65 nM VE resulted in an apoptotic phenotype similar to that produced by compounds that interfere primarily with homeostasis of cellular ions, such as Ca<sup>2+</sup>, Na<sup>+</sup>, and K<sup>+</sup>. This observation led us to hypothesize that VE potentially impacts the functionality of intracellular membrane systems (Figure 2A). VE-resistant U2OS cells (U2OS-R), which are 10-fold less sensitive to VE than the parental U2OS cells, were screened out and used for RNA sequencing (RNA-seq). Differentially expressed genes were clustered and were then subjected to KEGG analysis. The lysosome pathway was the most heavily enriched with differentially expressed genes—approximately 30 lysosome-associated genes were markedly upregulated in U2OS-R cells (Figure 2B)—suggesting that the interference of VE with lysosomes was potentially related to its cytotoxic effects.

For further target identification via chemical proteomics (Li et al., 2013), we designed a VE-derived photoactive chemical probe, VE-P, by introducing a diazirine with a terminal alkyne moiety at the hydroxyamino position (Figure 2C). Promisingly, VE-P maintained favorable bioactivity, with an IC<sub>50</sub> of 110.5 nM in HL-60 cells, in which VE had an IC<sub>50</sub> of 25 nM. Through rhodamine-azide labeling, VE-P was observed to localize in the cytoplasm and to colocalize primarily with lysosomes labeled with LysoTracker red but not with the endoplasmic reticulum or mitochondria (Figure 2D). These data thus strongly suggest that VE may directly target lysosomes.

### VE Targets the v-H<sup>+</sup> ATPase Subunit ATP6V1G1

We next sought to identify the cellular target of VE using a chemical proteomic approach with a click chemistry-based strategy (Li et al., 2013). U2OS cell lysates were incubated with either VE-P or a negative control probe (NP). After 20 min of UV light exposure (365 nm), Cu(I) salt catalyzed a [3 + 2] azide-alkyne cycloaddition with biotin-azide used to biotinylate the probe-target complexes. The biotinylated complexes were then pulled down with streptavidin beads and analyzed by liquid chromatography-tandem mass spectrometry (Figure S2A; Table S2). Differential lysosomal proteins specific to VE-P-treated relative to NP-treated samples were subjected to gene ontology analysis. The top molecular function term was proton-transporting ATPase activity, rotational mechanism (GO:0046961), in which lysosome-specific v-ATPase subunits were clustered (Table S3).

We further individually verified the interactions between VE-P and 15 subunits of the v-ATPase. We transfected 293T cells with HA-tagged v-ATPase subunits and subjected them to a click reaction, and the ATP6V1B2, ATP6V1D, and ATP6V1G subunits were pulled down by VE-P. VE-P showed robust interaction with the ATP6V1G subunit, as indicated by the higher ratio of precipitated ATP6V1G than the other subunits to input (Figures 3A and S2B). ATP6V1G1 is ubiquitously expressed, while ATP6V1G2 and ATP6V1G3 are uniquely expressed in brain and

kidney tissue, respectively. More importantly, VE pretreatment blocked VE-P labeling of ATP6V1G1 but not ATP1V1B2 or ATP6V1D in a competitive binding assay (Figure S2C). Moreover, via immunoprecipitation with an anti-ATP6V1G1 antibody, we found that VE-P bound to endogenous ATP6V1G1 in U2OS cells (Figure S2D). We further evaluated v-ATPase activity *in vitro* by measuring the rate of ATP hydrolysis (Figure 3B) and rate of acidification (Figure 3C) of isolated lysosomes upon treatment with VE or the known v-ATPase inhibitor bafilomycin A1 (Baf A1). VE showed substantial inhibition of v-ATPase activity at 10 nM *in vitro*, as did Baf A1, although to a lesser extent (Figures 3B and 3C).

### Antiproliferative Activity by VE Is Mediated via Interaction with ATP6V1G1

To determine the specific motifs and residues that mediate binding between VE and ATP6V1G1, we generated a series of plasmids with amino acid deletions in ATP6V1G1 to map the exact VE-binding motif within ATP6V1G1. ATP6V1G1<sup>Δ90–99</sup> and ATP6V1G1<sup>Δ100–109</sup> exhibited negligible interactions with VE-P, while ATP6V1G1 with deletions spanning amino acids 1–90 retained a robust interaction with VE-P, thus suggesting that amino acids 90–110 within ATP6V1G1 most likely include the VE-V1G1 interface (Figure S2E). Close scrutiny of the protein sequence alignment results suggested that leucine residue 99 and cysteine residue 104 are critical residues for interaction, since they are conserved among the three V1G isoforms that can bind VE-P (Figure 3A). We then generated knockin A375 and U2OS cells that stably expressed the ATP6V1G1 variants (Figure S2F) and found that the introduction of single or double mutations at L99S and C104Y impaired the interaction with VE-P (Figure 3D).

We then sought to determine whether these ATP6V1G1 mutations would maintain protein functionality but confer resistance to VE. Indeed, A375 and U2OS cells expressing any of the ATP6V1G1 mutants exhibited increased resistance to VE, as indicated by the decrease in propidium iodide-positive cells (Figure 3E) compared with that among ATP6V1G1<sup>WT</sup> cells and especially double-mutant ATP6V1G1<sup>L99S/C104Y</sup> cells. Notably, introduction of any of the three ATP6V1G1 mutants did not result in an observable change in v-ATPase activity or v-ATPase assembly, as indicated by LysoSensor staining (Figure 3F, top) and immunoprecipitation (Figure S2G), respectively. Importantly, the ATP6V1G1 mutants also conferred resistance to VE-induced v-ATPase activity blockade (Figure 3F). Together, these results clearly indicate that VE specifically targets the v-H<sup>+</sup> ATPase via its ATP6V1G1 subunit, which accounts for its anti-proliferative activity.

The v-ATPase has been reported to play a critical role in pathological conditions, such as cancers. ATP6V1G is a component of the peripheral stalk of the v-ATPase. Knocking down ATP6V1G1 in A375 and U2OS cells by transfection of

indicates the magnitude of the difference: blue, increase; yellow, decrease; black, no difference.) The right panel shows compounds that yield cytological profiles similar to VE at the indicated concentration (μM).

(B) The lysosome pathway is enriched in VE-resistant U2OS cells. Upregulated genes in VE-resistant U2OS cells compared with wild-type cells were clustered for KEGG enrichment analysis.

(C) Structures of VE-P. The IC<sub>50</sub> value for VE-P was tested in HL-60 cells.

(D) VE-P localizes to lysosomes in HL-60 cells. HL-60 cells were treated with 500 nM VE-P for 1 h followed by a “click” reaction with rhodamine-N3. Lysosomes, mitochondria, and endoplasmic reticulum (ER) were labeled by LysoTracker red, Mito-Tracker, or ER-Tracker, respectively. Scale bars, 8 μm.

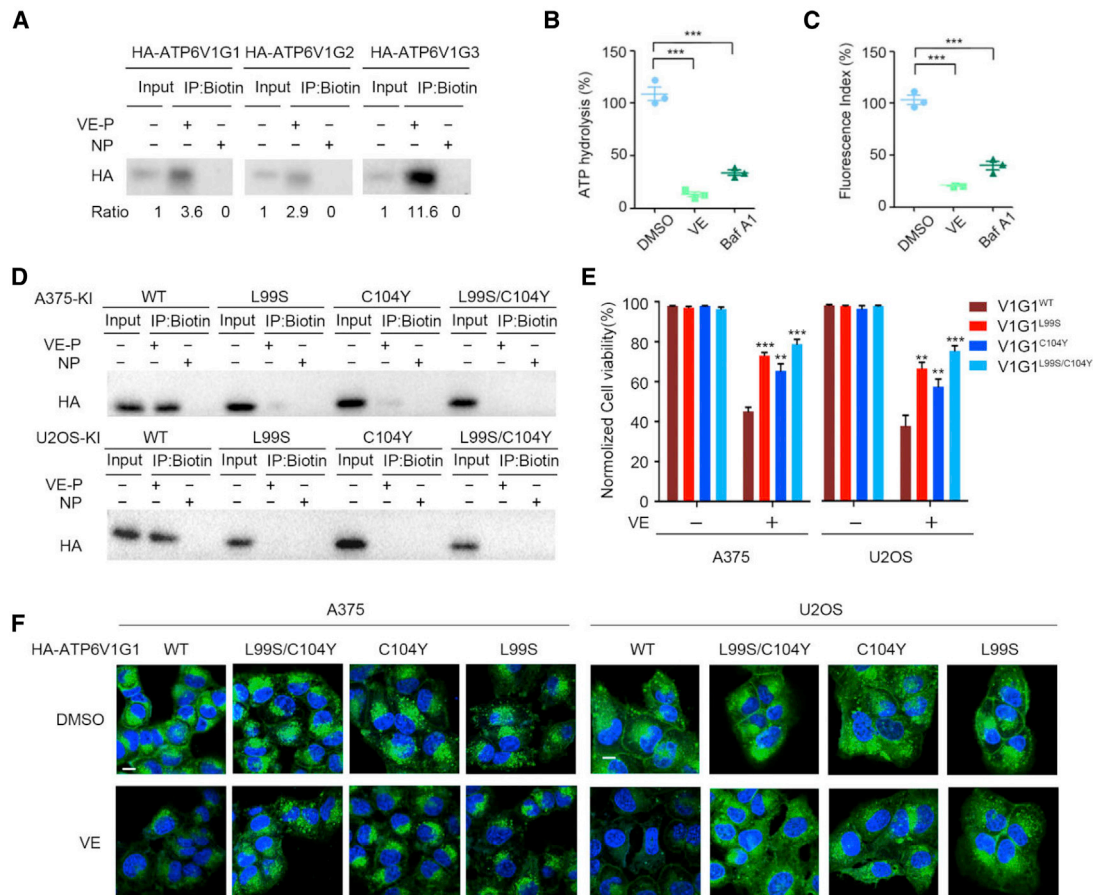


**Figure 3. VE Targets Subunit V1G of v-ATPase**

(A) VE-P has specific interaction with ATP6V1G1-3 in HA-ATP6V1G-expressing 293T cells. Cell lysates were treated with VE-P or NP followed by click reaction with biotin-N3. Cell lysate was pulled down by avidin-agarose beads and subjected to western blot.  
 (B) VE inhibits v-ATPase activity *in vitro*. Purified lysosomes were incubated with 10 nM VE or Baf A1 for 1 h and ATP hydrolysis rate was measured using a coupled spectrophotometric method by continuously recording OD341. Statistical results were graphed as mean  $\pm$  SEM, n = 3, p value by Student's t test. \*\*\*p < 0.001.  
 (C) VE suppresses lysosomal acidification *in vitro*. Lysosomes loaded with fluorescein isothiocyanate (FITC)-dextran were purified and then incubated with 10 nM VE or Baf A1 for 1 h. Fluorescence of FITC was recorded. Statistical results were graphed as mean  $\pm$  SEM, n = 3, p value by Student's t test. \*\*\*p < 0.001.  
 (D) ATP6V1G1 mutants regarding L99 and C104 abolish interaction between V1G1 and VE. HA-ATP6V1G1<sup>L99S/C104Y</sup>, HA-ATP6V1G1<sup>L99S</sup>, and HA-ATP6V1G1<sup>C104Y</sup> were introduced into U2OS and A375 cells. Cell lysates were treated with VE-P or NP followed by click reaction and western blot.  
 (E and F) ATP6V1G1 mutants regarding L99 and C104 confer resistance to VE-induced cell death and v-ATPase activity repression. HA-ATP6V1G1<sup>L99S/C104Y</sup>, HA-ATP6V1G1<sup>L99S</sup>, and HA-ATP6V1G1<sup>C104Y</sup> were introduced into U2OS and A375 cells. (E) Cells were treated with 200 nM VE for 24 h. Cell viability were quantified by flow cytometry using propidium iodide staining. Statistical results were graphed as mean  $\pm$  SEM, n = 3, p value by Student's t test. \*\*\*p < 0.001, \*\*p < 0.01. (F) v-ATPase activity was demonstrated by LysoSensor staining. The knocked in cells were treated with 200 nM VE for 2 h followed by LysoSensor and Hoechst staining. Scale bars, 10  $\mu$ m.  
 See also Figures S2 and S3 and Tables S2 and S3.

shATP6V1G1 significantly reduced the number of colonies formed (Figure S3A). Moreover, analysis of skin cutaneous melanoma (Figure S3B) and acute myeloid leukemia (Figure S3C) datasets in The Cancer Genome Atlas database revealed that a high expression level of ATP6V1G1/ATP6V1G2/ATP6V1G3 was associated with poor patient survival rates (Gao et al., 2013; Ley et al., 2013). These findings suggest that ATP6V1G is associated with cancer progression.

### VE Inhibits mTORC1 Signaling by Targeting ATP6V1G1

Lysosomes serve as a scaffolding platform for amino acid-mediated mTORC1 activation (Bar-Peled et al., 2012; Kim et al., 2008; Zoncu et al., 2011). The v-ATPase engages in

amino acid-sensitive interactions with the Regulator-Rag complex and, through a poorly understood mechanism, converts the Rag GTPase to its active nucleotide-bound state (RagA/B<sup>GTP</sup> and RagC/D<sup>GDP</sup>) (Anandapadmanaban et al., 2019; Lawrence et al., 2019; Shen et al., 2019), thereby allowing the recruitment of mTORC1 to the lysosomal surface (Rogala et al., 2019; Saxton and Sabatini, 2017). VE has been reported to attenuate mTORC1 signaling, although the mechanism was not explicitly defined (Yoshimura et al., 2015). We then verified the phosphorylation levels of mTORC1 substrates in HL60 cells. Unlike the allosteric mTORC1 inhibitor rapamycin, VE exhibited substantial inhibition of p-S6K as well as p-4EBP1 at concentrations of 10–200 nM (Figure 4A). In addition, VE

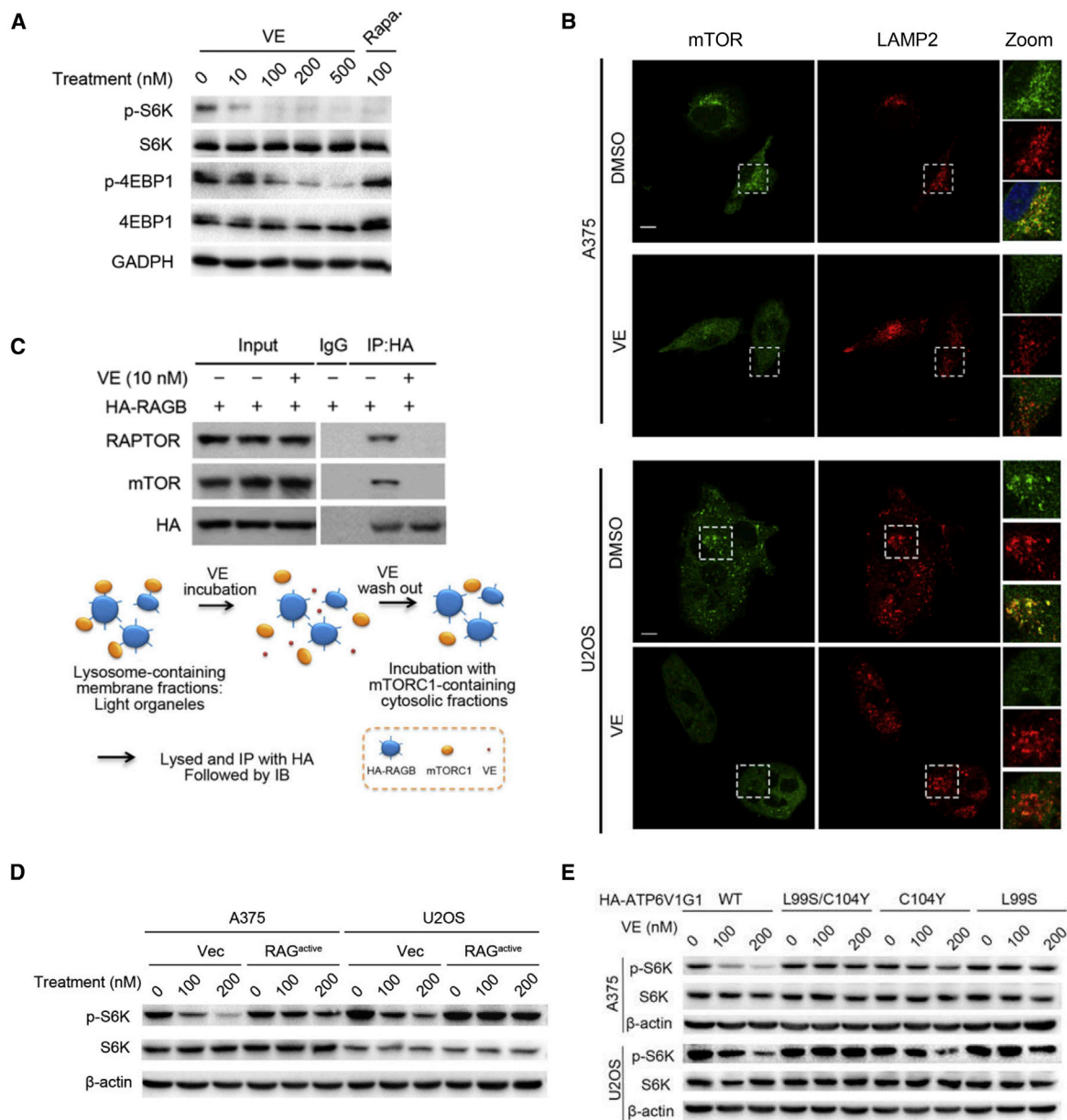


**Figure 4. VE Attenuates mTORC1 via ATP6V1G1**

(A) VE inhibits mTORC1 downstream substrates. HL-60 cells were treated with VE and rapamycin as indicated. Cell lysates were subjected to western blot. (B) VE induces mTOR disassociation from lysosome membrane. U2OS and A375 cells were treated with 200 nM VE for 2 h and stained with mTOR and LAMP2 antibodies. Scale bars, 20 μm. (C) VE blocks interaction between mTORC1 and RAGB *in vitro*. Lysosome-containing membrane fractions in HA-RAGB stably expressing mouse embryonic fibroblasts were isolated and incubated with 10 nM VE for 1 h. VE was washed off and light organelles were further incubated with mTORC1-containing cytosolic fractions, finally followed by immunoprecipitation and western blot. (D) Active form of RAG (RAG<sup>active</sup>, consisting of HA-RagA GTP(Q66L), HA-RagB GTP(Q99L), HA-RagC GDP(S75L), HA-RagD GDP(S77L)), or control vector were stably transfected into A375 and U2OS cells. RAG<sup>active</sup>-transfected A375 and U2OS cells were resistant to VE-induced mTORC1 downregulation. Cells were treated with VE for 2 h as indicated. Cell lysates were examined by western blot. (E) ATP6V1G1 mutants regarding L99 and C104 confer resistance to VE-induced mTORC1 inhibition. Cell lysates were subjected to western blot. See also [Figure S4](#).

efficiently attenuated the phosphorylation of most of the tested mTORC1 downstream substrates, including p-4EBP1, p-mTOR<sup>S2448</sup>, p-mTOR<sup>S2481</sup>, p-Rictor, p-ULK1, and p-Grb 10, at low concentrations ranging from 50 to 500 nM ([Figure S4A](#)).

Collectively, these findings indicate that VE is a highly potent modulator of mTORC1 signaling.

Next, we examined the subcellular location of mTOR upon VE treatment. As shown in [Figure 4B](#), mTOR dissociated from the

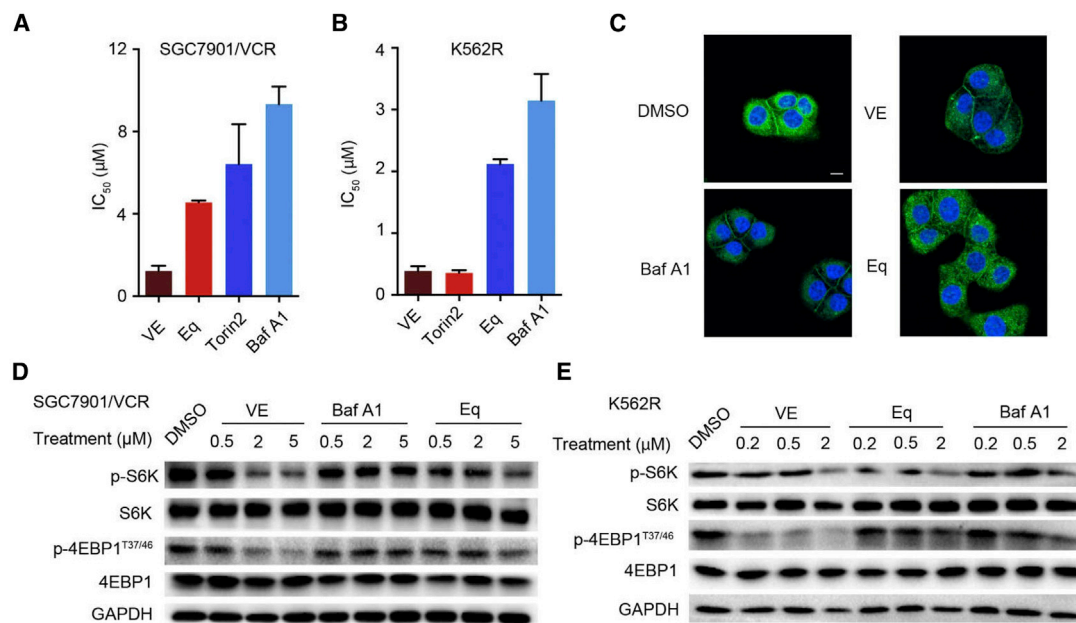


**Figure 5. VE Exhibits the Most Potent v-ATPase and mTORC1 Inhibition in MDR Cancer Cells**

(A) IC<sub>50</sub> values of indicated compounds against SGC7901/VCR tested by MTS assay. Data are represented as means ± SEM, n = 3.

(B) IC<sub>50</sub> values of indicated compounds against K562R tested by MTS assay. Data are represented as means ± SEM, n = 3.

(C) The inhibitory efficacy of VE, Baf A1, and Eq on v-ATPase activity. SGC7901/VCR cells were treated with indicated compounds at 2 μM for 2 h followed by LysoSensor and Hoechst staining. Scale bar, 10 μm.

(D and E) The inhibitory activity of VE, Baf A1 and Eq on mTORC1 signaling. SGC7901/VCR cells (D) and K562R cells (E) were incubated with VE, Eq, and Baf A1 as indicated for 2 h. Cell lysates were subjected to western blot using appropriate antibodies.

See also Figure S5.

lysosomal surface in U2OS cells. Then, the effect of VE treatment on lysosome binding with mTOR was investigated in a cell-free system that recapitulates the amino acid-induced binding of mTORC1 to Rag GTPases on the lysosomal surface (Zoncu et al., 2011). Lysosomes purified from mouse embryonic fibroblasts stably expressing HA-RagB were treated with VE, washed, and incubated with mTORC1-containing cytosolic fractions. After incubation, lysosomes were lysed and immunoprecipitated with an anti-HA antibody (Figure 4C). The resulting immunoblots further confirmed that both mTOR and RAPTOR, components of the mTORC1 complex, dissociated from lysosomes upon VE treatment (Figure 4C). We further generated cells stably expressing RagA/B<sup>GTP</sup> and RagC/D<sup>GDP</sup> (labeled RAG<sup>active</sup>), in which mTORC1 was constitutively activated and recruited to the lysosomal surface (Figure S4B). Both A375 and U2OS RAG<sup>active</sup> cells showed higher resistance to VE-induced mTORC1 downregulation (Figure 4D) than their corresponding parental cells. These results demonstrate that VE downregulates mTORC1 signaling via the Rag-dependent lysosomal machinery. Importantly, the ATP6V1G1<sup>L99S</sup> and ATP6V1G1<sup>C104Y</sup> mutations also conferred resistance to VE-induced downregulation of mTORC1 signaling (Figure 4E), indicating that VE-mediated downregulation of mTORC1 signaling is produced through targeting of ATP6V1G1.

### VE Kills MDR Cancer Cells by Evident Inhibition of Both the v-ATPase and mTORC1

Both mTORC1 and the v-ATPase are reported to enhance the MDR phenotype by reprogramming metabolism (Alexa-Stratulat

et al., 2019; Martin et al., 2014; VanderWeele and Rudin, 2005), upregulating MDR1 (Aldonza et al., 2015), or modulating the pH gradient across the lysosome/cytosol barrier as well as the intra/extracellular barrier (Stransky et al., 2016). The superior ability of VE to inhibit mTOR (Figures 4A and S4A) and block v-ATPase activity (Figures 3B and 3C) might account for its potent antitumor activity against MDR cancer cells.

We evaluated the antiproliferative activities of VE, as well as the well-known v-ATPase inhibitors Baf A1 (Bowman et al., 2004) and electrophilic quinazoline (Eq) (Chen et al., 2017) and the ATP-competitive mTORC1/mTORC2 inhibitor torin2 (Liu et al., 2011), against SGC7901/VCR cells. As shown in Figure 5A, all tested molecules exhibited IC<sub>50</sub> values of less than 10 μM in SGC7901/VCR cells, much lower than those of other clinical agents shown in Figure 1A. This result was further verified in K562R cells, in which the IC<sub>50</sub> values ranged from 0.3 to 3 μM (Figure 5B), much lower than those of Taxol and vincristine (Figure 1C). Taken together, these results indicate that, among the tested agents, VE showed the strongest antiproliferative ability against MDR cells.

Since V1G-targeted VE showed 3- to 10-fold higher antiproliferative activity than the well-known v-ATPase inhibitors VOC-targeted Baf A1 (Bowman et al., 2004) and V1A-targeted Eq (Chen et al., 2017) (Figure S5A), we sought to determine whether modulating different subunits of the v-ATPase would have different benefits. We first examined the lysosomal pH in MDR cells by LysoSensor staining and found that the capability of VE to inhibit v-ATPase activity was equivalent to that of Baf A1. Eq also suppressed v-ATPase activity, albeit to a lesser extent than VE

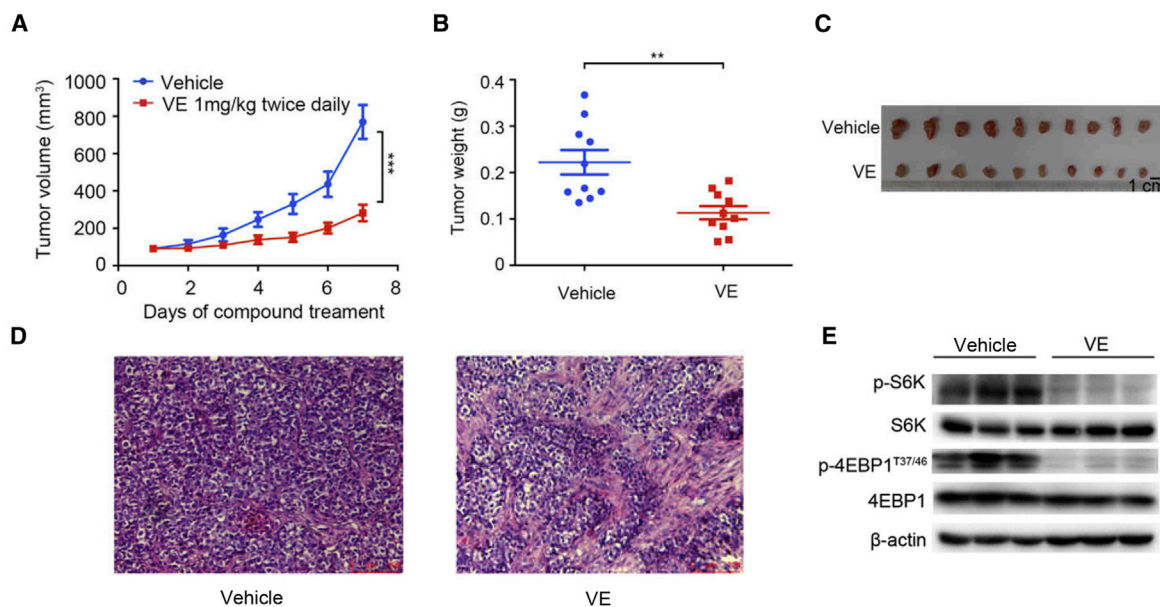


**Figure 6. VE Inhibits Tumor Growth in MDR Cancer Xenograft Model**

(A–C) Tumors (n = 10) of SGC7901/VCR xenograft model were harvested at day 7. Tumor volume (A) and weights (B) were measured. Photograph of tumors is shown (C). Data are represented as mean ± SEM, p value by Student's t test. \*\*\*p < 0.001, \*\*p < 0.01.

(D) Hematoxylin and eosin staining of tumor samples. Scale bar, 50 μm.

(E) Immunoblot analysis of expression and phosphorylation of S6K and 4EBP1.

See also Figure S6.

(Figures 5C and S5B). Moreover, VE efficiently attenuated the phosphorylation of the mTORC1 downstream substrates p-S6K and p-4EBP1. However, cells treated with Eq showed comparable levels of decreased phosphorylation at 3- to 10-fold higher concentrations than cells treated with VE, and Baf A1 showed a negligible effect on the phosphorylation of these substrates (Figures 5D and 5E). The distinctly different inhibitory effects of these v-ATPase inhibitors on v-ATPase and mTORC1 suggest that the suppression of mTORC1 signaling is not consistent with the inhibition of v-ATPase activity. Pharmacological targeting of the v-ATPase V1G subunit might be the most efficient approach to inhibit both v-ATPase activity and mTORC1 signaling.

### VE Suppresses MDR Cancer Progression *In Vivo*

Considering the superior activity of VE against MDR cancer cells, we finally investigated the *in vivo* antitumor activity of VE in a xenograft mouse model established with SGC7901/VCR cells. At a low dose of 1 mg kg<sup>-1</sup> twice daily for 7 days, VE substantially repressed tumor growth (Figures 6A–6C) without significant body weight loss or gross signs of toxicity (Figure S6). Hematoxylin and eosin staining indicated that VE potently induced cell death (Figure 6D). Furthermore, mTORC1 signaling was abrogated by VE, as demonstrated by dephosphorylation of S6K and 4EBP1 (Figure 6E). Taken together, these results indicate that VE exhibits profound antitumor efficacy *in vivo* against MDR tumors.

### DISCUSSION

Alterations in the pH gradient and cellular metabolism have been recognized as hallmarks of cancer, and the v-ATPase and mTOR

act as central regulators in these vital cellular processes, respectively (Saxton and Sabatini, 2017; Stransky et al., 2016). As a proton pump, the v-ATPase aids the development of drug resistance via lysosomal sequestration of hydrophobic weak base chemotherapeutics and acidification of the extracellular environment (Stransky et al., 2016). Moreover, the v-ATPase functions in crucial cellular signal transduction pathways that promote cancer cell survival and progression, particularly the Wnt, Notch, and mTOR pathways (Stransky et al., 2016). mTORC1 signaling is hyperactivated in many types of cancer (Rodrik-Outmezguine et al., 2016) and is reported to participate in the development of MDR through multiple mechanisms, such as glycometabolic adaptation (Zhang et al., 2017). Moreover, aberrations in the PI3K/Akt/mTOR pathway upregulate the MDR1 gene in MDR breast (Martin et al., 2014) and lung (Aldonza et al., 2015) cancers. In this study, we showed that VE, an inhibitor of the v-ATPase peripheral stalk, exhibited excellent antiproliferative activity against MDR cancer cells *in vitro* and *in vivo* via substantial inhibition of both v-ATPase activity and mTORC1 signaling. Our results suggest that inhibition of both mTORC1 and the v-ATPase by a new v-ATPase inhibitor is an attractive strategy for combating cancer, especially MDR cancer, thus killing two birds with one stone.

Although the v-ATPase acts upstream of mTORC1 on the lysosomal surface, the distinctly different outcomes of VE, Eq, and Baf A1 on v-ATPase and mTORC1 inhibition suggest that the suppression of mTORC1 signaling is not consistent with the inhibition of v-ATPase activity. These data support the idea that the conformational rearrangement of the v-ATPase, not the pH gradient across the lysosomal membrane, causes the dissociation of mTORC1 from Rags (Zoncu et al., 2011). This finding is further supported

by a recent report of the v-ATPase activator EN6. By covalently targeting cysteine 277 of ATP6V1A, EN6 not only profoundly stimulates v-ATPase activity but also inhibits mTORC1 signaling and subsequently induces autophagy (Chung et al., 2019). V1G is a subunit of the peripheral stalk, and its proximity to Rags might facilitate allosteric regulation of mTORC1, which explains why VE exhibited the strongest inhibitory effects on mTORC1 among the tested v-ATPase inhibitors. Moreover, VE exhibited tissue specificity for cancers, such as leukemia, lymphoma, and melanoma, in which poor outcomes were associated with high expression levels of ATP6V1G. These results suggest that pharmacological targeting of the v-ATPase via the V1G subunit provides a favorable therapeutic approach for cancers with dysregulated v-ATPase or mTOR signaling, such as MDR cancers.

Natural products with privileged scaffolds hold great promise for molecular probe design and drug development; however, elucidation of their molecular targets remains a rate-limiting step (Farha and Brown, 2016; Pan et al., 2016). Here, we provided a valid and intuitive approach combining click chemistry-based proteomics with cytological profiling to facilitate target identification. We discovered that the natural cyclodepsipeptide VE interacts with the previously untargeted v-ATPase subunit ATP6V1G at the leucine 99 and cysteine 104 residues. VE can clearly serve as a versatile probe for investigating v-ATPase and mTORC1 biology, as well as constitute a lead compound for the development of anticancer therapies, especially for MDR cancers.

## SIGNIFICANCE

**Multidrug resistance in cancer remains a major obstacle for successful chemotherapeutic treatment. Although numerous mechanisms have been shown to be involved in the development of multidrug resistance, no clinically satisfactory therapeutic interventions have been reported to date. Therefore, the search for new strategies and identification of new chemical entities for combating multidrug-resistant (MDR) are urgently needed. In this study, we identified a natural product, the cyclodepsipeptide verucopeptin, with notable antitumor potency against MDR cells. A detailed mechanistic investigation revealed that verucopeptin strongly inhibited both v-ATPase activity and mTORC1 signaling by targeting ATP6V1G, leading to substantial pharmacological efficacy against MDR cancer cells *in vitro* as well as in a xenograft mouse model *in vivo*. Our results demonstrate that targeting the v-ATPase via subunit V1G provides a unique approach for modulating v-ATPase and mTORC1 signaling with great potential for the development of therapeutics against MDR cancers.**

## STAR★METHODS

Detailed methods are provided in the online version of this paper and include the following:

- KEY RESOURCES TABLE
- RESOURCE AVAILABILITY
  - Lead Contact
  - Materials Availability
  - Data and Code Availability

## ● EXPERIMENTAL MODEL AND SUBJECT DETAILS

- Cell Culture
- Mice

## ● METHOD DETAILS

- Fermentation and Extraction
- Large Panel of Cancer Cells Profiling for VE
- Cell Viability Assay
- Cytological Profiling
- Immunoblotting
- Immunoprecipitation
- Immunofluorescence Staining
- Annexin V-FITC/PI Assay
- Inducing of VE Resistance in U2OS Cells
- Knock down Experiments
- Transient Transfection and Lentivirus Infection
- Chemical Labelling of VE-P and Fluorescence Microscopy
- Pull-down Assay and LC-MS/MS Analysis
- Characterization of Verucopeptin (VE)
- Synthesis of VE-P, NP and Eq
- Isolation of Light Organelles
- Purification of Lysosomes
- Measurement of V-ATPase Activity *In Vitro*
- In Vivo Assay
- Hematoxylin and Eosin Staining

## ● QUANTIFICATION AND STATISTICAL ANALYSIS

## SUPPLEMENTAL INFORMATION

Supplemental Information can be found online at <https://doi.org/10.1016/j.chembiol.2020.06.011>.

## ACKNOWLEDGMENTS

We thank Dr. C. Xie and Y. Wu for help with mass spectrometry experiments and analysis, and H. Huang for help with NMR experiments. K562R cells were given by Prof. R. Ren in Shanghai Institute of Hematology, Ruijin Hospital, Shanghai Jiao Tong University School of Medicine, Shanghai, China. This work was supported by grants from the National Key R&D Program and the National Natural Science Foundation of China (nos. 2017YFA0504504, 2016YFA0502001, 91853203, U1405223, 81422045, and 81661138005 to X.D., 81603131 to L.L., 21402165 to W.H., and 81903491 to Y.W.), the Fundamental Research Funds for the Central Universities of China (nos. 20720190101 and 20720200008 to X.D., 20720170067 to L.L., and 20720190113 to D.Z.), and the Program of Introducing Talents of Discipline to Universities (111 Project, B06016).

## AUTHOR CONTRIBUTIONS

X.D. conceived the project. Y.W., Z.H., Q.X., Y.S., and A.W. performed VE purification and structure determination. W.H. conceived and performed chemical synthesis of VE-P. X.D. and L.L. designed the biology experiments. L.Z., Y.-L.W., L.Y., C.-S.Z., M.L., W.L., and X.W. performed the biological experiments, and acquired and analyzed data. W.M.B. and M.S.J. performed cytological profiling and data analysis. A.D., P.G., C.H.B., and J.Z. performed large-scale CMT profiling and data analysis. X.D., L.L., G.L., J.-H.G., L.C., H.-R.W., D.Z., S.-C.L., and J.Z. contributed to analysis and interpretation of biological data. Y.W., L.L., and X.D. co-wrote the paper. All authors read and approved the final manuscript.

## DECLARATION OF INTERESTS

The authors declare no conflict of interest.

Received: April 1, 2020  
Revised: June 3, 2020  
Accepted: June 15, 2020  
Published: July 9, 2020

## REFERENCES

- Aldonza, M.B., Hong, J.Y., Bae, S.Y., Song, J., Kim, W.K., Oh, J., Shin, Y., Lee, S.H., and Lee, S.K. (2015). Suppression of MAPK signaling and reversal of mTOR-dependent MDR1-associated multidrug resistance by 21 $\alpha$ -methylmelaniodiol in lung cancer cells. *PLoS One* *10*, e0127841.
- Alexa-Stratulat, T., Pešić, M., Gašparović, A.Č., Trougakos, I.P., and Riganti, C. (2019). What sustains the multidrug resistance phenotype beyond ABC efflux transporters? Looking beyond the tip of the iceberg. *Drug Resist. Updat.* *46*, 100643.
- Anandapadamanaban, M., Masson, G.R., Perisic, O., Berndt, A., Kaufman, J., Johnson, C.M., Santhanam, B., Rogala, K.B., Sabatini, D.M., and Williams, R.L. (2019). Architecture of human Rag GTPase heterodimers and their complex with mTORC1. *Science* *366*, 203–210.
- Arai, S., Saijo, S., Suzuki, K., Mizutani, K., Kakinuma, Y., Ishizuka-Katsura, Y., Ohsawa, N., Terada, T., Shirouzu, M., Yokoyama, S., et al. (2013). Rotation mechanism of *Enterococcus hirae* V-1-ATPase based on asymmetric crystal structures. *Nature* *493*, 703–707.
- Bar-Peled, L., Schweitzer, L.D., Zoncu, R., and Sabatini, D.M. (2012). Regulator is a GEF for the Rag GTPases that signal amino acid levels to mTORC1. *Cell* *150*, 1196–1208.
- Bonam, S.R., Wang, F.J., and Muller, S. (2019). Lysosomes as a therapeutic target. *Nat. Rev. Drug Discov.* *18*, 923–948.
- Bowman, E.J., Graham, L.A., Stevens, T.H., and Bowman, B.J. (2004). The bacillomycin/concanamycin binding site in subunit c of the V-ATPases from *Neurospora crassa* and *Saccharomyces cerevisiae*. *J. Biol. Chem.* *279*, 33131–33138.
- Chen, Y.C., Backus, K.M., Merkulova, M., Yang, C., Brown, D., Cravatt, B.F., and Zhang, C. (2017). Covalent modulators of the vacuolar ATPase. *J. Am. Chem. Soc.* *139*, 639–642.
- Chung, C.Y., Shin, H.R., Berdan, C.A., Ford, B., Ward, C.C., Olzmann, J.A., Zoncu, R., and Nomura, D.K. (2019). Covalent targeting of the vacuolar H<sup>(+)</sup>-ATPase activates autophagy via mTORC1 inhibition. *Nat. Chem. Biol.* *15*, 776–785.
- Farha, M.A., and Brown, E.D. (2016). Strategies for target identification of antimicrobial natural products. *Nat. Prod. Rep.* *33*, 668–680.
- Gao, J.J., Aksoy, B.A., Dogrusoz, U., Dresdner, G., Gross, B., Sumer, S.O., Sun, Y.C., Jacobsen, A., Sinha, R., Larsson, E., et al. (2013). Integrative analysis of complex cancer genomics and clinical profiles using the cBioPortal. *Sci. Signal.* *6*, p11.
- Garnett, M.J., Edelman, E.J., Heidorn, S.J., Greenman, C.D., Dastur, A., Lau, K.W., Greninger, P., Thompson, I.R., Luo, X., Soares, J., et al. (2012). Systematic identification of genomic markers of drug sensitivity in cancer cells. *Nature* *483*, 570–575.
- Gillet, J.P., and Gottesman, M.M. (2010). Mechanisms of multidrug resistance in cancer. *Methods Mol. Biol.* *596*, 47–76.
- Hale, K.J., Manaviyar, S., and George, J. (2010). Total synthesis of (+)-A83586C, (+)-kettapeptin and (+)-azinothricin: powerful new inhibitors of beta-catenin/TCF4 and E2F-mediated gene transcription. *Chem. Commun.* *46*, 4021–4042.
- Holohan, C., Van Schaeybroeck, S., Longley, D.B., and Johnston, P.G. (2013). Cancer drug resistance: an evolving paradigm. *Nat. Rev. Cancer* *13*, 714–726.
- Jia, H., Yang, Q., Wang, T., Cao, Y., Jiang, Q.Y., Ma, H.D., Sun, H.W., Hou, M.X., Yang, Y.P., and Feng, F. (2016). Rhamnetin induces sensitization of hepatocellular carcinoma cells to a small molecular kinase inhibitor or chemotherapeutic agents. *Biochim Biophys Acta* *1860*, 1417–1430.
- Kim, E., Goraksha-Hicks, P., Li, L., Neufeld, T.P., and Guan, K.L. (2008). Regulation of TORC1 by Rag GTPases in nutrient response. *Nat. Cell Biol.* *10*, 935–945.
- Kumar, A., and Jaitak, V. (2019). Natural products as multidrug resistance modulators in cancer. *Eur. J. Med. Chem.* *176*, 268–291.
- Lawrence, R.E., Fromm, S.A., Fu, Y., Yokom, A.L., Kim, D.J., Thelen, A.M., Young, L.N., Lim, C.Y., Samelson, A.J., Hurley, J.H., et al. (2019). Structural mechanism of a Rag GTPase activation checkpoint by the lysosomal folliculin complex. *Science* *366*, 971–977.
- Ley, T.J., Miller, C., Ding, L., Raphael, B.J., Mungall, A.J., Robertson, A.G., Hoadley, K., Triche, T.J., Laird, P.W., Baty, J.D., et al. (2013). Genomic and epigenomic landscapes of adult de novo acute myeloid leukemia. *New Engl. J. Med.* *368*, 2059–2074.
- Li, Z.Q., Hao, P.L., Li, L., Tan, C.Y.J., Cheng, X.M., Chen, G.Y.J., Sze, S.K., Shen, H.M., and Yao, S.Q. (2013). Design and synthesis of minimalist terminal alkyne-containing diazirine photo-crosslinkers and their incorporation into kinase inhibitors for cell- and tissue-based proteome profiling. *Angew. Chem. Int. Ed.* *52*, 8551–8556.
- Liberman, R., Bond, S., Shainheit, M.G., Stadecker, M.J., and Forgac, M. (2014). Regulated assembly of vacuolar ATPase is increased during cluster disruption-induced maturation of dendritic cells through a phosphatidylinositol 3-kinase/mTOR-dependent pathway. *J. Biol. Chem.* *289*, 1355–1363.
- Liu, Q., Wang, J., Kang, S.A., Thoreen, C.C., Hur, W., Ahmed, T., Sabatini, D.M., and Gray, N.S. (2011). Discovery of 9-(6-aminopyridin-3-yl)-1-(3-(trifluoromethyl)phenyl)benzo[h][1,6]naphthyridin-2(1H)-one (Torin2) as a potent, selective, and orally available mammalian target of rapamycin (mTOR) inhibitor for treatment of cancer. *J. Med. Chem.* *54*, 1473–1480.
- Longley, D.B., and Johnston, P.G. (2005). Molecular mechanisms of drug resistance. *J. Pathol.* *205*, 275–292.
- Maehr, H., Liu, C.M., Palleroni, N.J., Smallheer, J., Todaro, L., Williams, T.H., and Blount, J.F. (1986). Microbial products. 8. Azinothricin, a novel hexadepsipeptide antibiotic. *J. Antibiot.* *39*, 17–25.
- Martin, H.L., Smith, L., and Tomlinson, D.C. (2014). Multidrug-resistant breast cancer: current perspectives. *Breast Cancer* *6*, 1–13.
- Montazami, N., Aghapour, M., Farajnia, S., and Baradaran, B. (2015). New insights into the mechanisms of multidrug resistance in cancers. *Cell Mol. Biol.* *61*, 70–80.
- Nakanishi, A., Kishikawa, J.I., Tamakoshi, M., Mitsuoka, K., and Yokoyama, K. (2018). Cryo EM structure of intact rotary H<sup>(+)</sup>-ATPase/synthase from *Thermus thermophilus*. *Nat. Commun.* *9*, 89.
- Newman, D.J., and Cragg, G.M. (2016). Natural products as sources of new drugs from 1981 to 2014. *J. Nat. Prod.* *79*, 629–661.
- Ning, N., Yu, Y., Wu, M., Zhang, R., Zhang, T., Zhu, C., Huang, L., Yun, C.H., Benes, C.H., Zhang, J., et al. (2018). A novel microtubule inhibitor overcomes multidrug resistance in tumors. *Cancer Res.* *78*, 5949–5957.
- Nishiyama, Y., Sugawara, K., Tomita, K., Yamamoto, H., Kamei, H., and Oki, T. (1993). Verucopiptin, a new antitumor antibiotic active against B16 melanoma. 1. Taxonomy, production, isolation, physicochemical properties and biological-activity. *J. Antibiot.* *46*, 921–927.
- Oelke, A.J., France, D.J., Hofmann, T., Wuitschik, G., and Ley, S.V. (2011). Piperazine acid-containing natural products: isolation, biological relevance and total synthesis. *Nat. Prod. Rep.* *28*, 1445–1471.
- Oot, R.A., Couoh-Cardel, S., Sharma, S., Stam, N.J., and Wilkens, S. (2017). Breaking up and making up: the secret life of the vacuolar H<sup>(+)</sup>-ATPase. *Protein Sci.* *26*, 896–909.
- Over, B., Wetzel, S., Grutter, C., Nakai, Y., Renner, S., Rauh, D., and Waldmann, H. (2013). Natural-product-derived fragments for fragment-based ligand discovery. *Nat. Chem.* *5*, 21–28.
- Pan, S.J., Zhang, H.L., Wang, C.Y., Yao, S.C.L., and Yao, S.Q. (2016). Target identification of natural products and bioactive compounds using affinity-based probes. *Nat. Prod. Rep.* *33*, 612–620.
- Rees, D.C., Johnson, E., and Lewinson, O. (2009). ABC transporters: the power to change. *Nat. Rev. Mol. Cell Biol.* *10*, 218–227.
- Robey, R.W., Pluchino, K.M., Hall, M.D., Fojo, A.T., Bates, S.E., and Gottesman, M.M. (2018). Revisiting the role of ABC transporters in multidrug-resistant cancer. *Nat. Rev. Cancer* *18*, 452–464.

- Rodrik-Outmezguine, V.S., Okaniwa, M., Yao, Z., Novotny, C.J., McWhirter, C., Banaji, A., Won, H., Wong, W., Berger, M., de Stanchina, E., et al. (2016). Overcoming mTOR resistance mutations with a new-generation mTOR inhibitor. *Nature* **534**, 272–276.
- Rogala, K.B., Gu, X., Kadir, J.F., Abu-Remalieh, M., Bianchi, L.F., Bottino, A.M.S., Dueholm, R., Niehaus, A., Overwijn, D., Fils, A.P., et al. (2019). Structural basis for the docking of mTORC1 on the lysosomal surface. *Science* **366**, 468–475.
- Roh, S.H., Stam, N.J., Hryc, C.F., Couch-Cardel, S., Pintilie, G., Chiu, W., and Wilkens, S. (2018). The 3.5-Å degrees CryoEM structure of nanodisc-reconstituted yeast vacuolar ATPase V-o proton channel. *Mol. Cell* **69**, 993–1004.
- Sakai, Y., Yoshida, T., Tsujita, T., Ochiai, K., Agatsuma, T., Saitoh, Y., Tanaka, F., Akiyama, T., Akinaga, S., and Mizukami, T. (1997). GE3, a novel hexadepesptide antitumor antibiotic, produced by *Streptomyces* sp. 1. Taxonomy, production, isolation, physico-chemical properties, and biological activities. *J. Antibiot.* **50**, 659–664.
- Saxton, R.A., and Sabatini, D.M. (2017). mTOR signaling in growth, metabolism, and disease. *Cell* **168**, 960–976.
- Schulze, C.J., Bray, W.M., Woerhmann, M.H., Stuart, J., Lokey, R.S., and Lington, R.G. (2013). Function-first\* lead discovery: mode of action profiling of natural product libraries using image-based screening. *Chem. Biol.* **20**, 285–295.
- Shao, E., and Forgac, M. (2004). Involvement of the nonhomologous region of subunit A of the yeast V-ATPase in coupling and in vivo dissociation. *J. Biol. Chem.* **279**, 48663–48670.
- Sharma, A., Lee, M.-G., Shi, H., Won, M., Arambula, J.F., Sessler, J.L., Lee, J.Y., Chi, S.-G., and Kim, J.S. (2018). Overcoming drug resistance by targeting cancer bioenergetics with an activatable prodrug. *Chem* **4**, 2370–2383.
- Shen, K., Rogala, K.B., Chou, H.T., Huang, R.K., Yu, Z., and Sabatini, D.M. (2019). Cryo-EM structure of the human FLCN-FNIP2-Rag-Ragulator complex. *Cell* **179**, 1319–1329 e1318.
- Silver, L.L. (2015). Natural products as a source of drug leads to overcome drug resistance. *Future Microbiol.* **10**, 1711–1718.
- Simon, S., Roy, D., and Schindler, M. (1994). Intracellular pH and the control of multidrug-resistance. *Proc. Natl. Acad. Sci. U S A* **91**, 1128–1132.
- Steinberg, B.E., Huynh, K.K., Brodovitch, A., Jabs, S., Stauber, T., Jentsch, T.J., and Grinstein, S. (2010). A cation counterflux supports lysosomal acidification. *J. Cell Biol.* **189**, 1171–1186.
- Stransky, L., Cotter, K., and Forgac, M. (2016). The function of V-ATPases in cancer. *Physiol. Rev.* **96**, 1071–1091.
- Sugawara, K., Toda, S., Moriyama, T., Konishi, M., and Oki, T. (1993). Verucopeptin, a new antitumor antibiotic active against B16 melanoma. 2. Structure determination. *J. Antibiot.* **46**, 928–935.
- Szakacs, G., Paterson, J.K., Ludwig, J.A., Booth-Genthe, C., and Gottesman, M.M. (2006). Targeting multidrug resistance in cancer. *Nat. Rev. Drug Discov.* **5**, 219–234.
- Trombetta, E.S., Ebersold, M., Garrett, W., Pypaert, M., and Mellman, I. (2003). Activation of lysosomal function during dendritic cell maturation. *Science* **299**, 1400–1403.
- VanderWeele, D.J., and Rudin, C.M. (2005). Mammalian target of rapamycin promotes vincristine resistance through multiple mechanisms independent of maintained glycolytic rate. *Mol. Cancer Res.* **3**, 635–644.
- Vukovic, V., and Tannock, I.F. (1997). Influence of low pH on cytotoxicity of paclitaxel, mitoxantrone and topotecan. *Br. J. Cancer* **75**, 1167–1172.
- Webb, B.A., Chimenti, M., Jacobson, M.P., and Barber, D.L. (2011). Dysregulated pH: a perfect storm for cancer progression. *Nat. Rev. Cancer* **11**, 671–677.
- Xu, Y., Zhou, P., Cheng, S., Lu, Q., Nowak, K., Hopp, A.K., Li, L., Shi, X., Zhou, Z., Gao, W., et al. (2019). A bacterial effector reveals the V-ATPase-ATG16L1 axis that initiates xenophagy. *Cell* **178**, 552–566.e20.
- Yoshimura, A., Nishimura, S., Otsuka, S., Hattori, A., and Takeya, H. (2015). Structure elucidation of verucopeptin, a HIF-1 inhibitory polyketide-hexapeptide hybrid metabolite from an actinomycete. *Org. Lett.* **17**, 5364–5367.
- Zhang, C.S., Jiang, B., Li, M.Q., Zhu, M.J., Peng, Y.Y., Zhang, Y.L., Wu, Y.Q., Li, T.Y., Liang, Y., Lu, Z.L., et al. (2014). The lysosomal v-ATPase-ragulator complex is a common activator for AMPK and mTORC1, acting as a switch between catabolism and anabolism. *Cell Metab.* **20**, 526–540.
- Zhang, C.S., Li, M.Q., Ma, T., Zong, Y., Cui, J.W., Feng, J.W., Wu, Y.Q., Lin, S.Y., and Lin, S.C. (2016). Metformin activates AMPK through the lysosomal pathway. *Cell Metab.* **24**, 521–522.
- Zhang, X.Y., Ai, Z.Y., Chen, J., Yi, J., Liu, Z.A., Zhao, H.S., and Wei, H.L. (2017). Glycometabolic adaptation mediates the insensitivity of drug-resistant K562/ADM leukaemia cells to adriamycin via the AKT-mTOR/c-Myc signalling pathway. *Mol. Med. Rep.* **15**, 1869–1876.
- Zhao, J.H., Benlekbir, S., and Rubinstein, J.L. (2015). Electron cryomicroscopy observation of rotational states in a eukaryotic V-ATPase. *Nature* **521**, 241–245.
- Zoncu, R., Bar-Peled, L., Efeyan, A., Wang, S.Y., Sancak, Y., and Sabatini, D.M. (2011). mTORC1 senses lysosomal amino acids through an inside-out mechanism that requires the vacuolar H<sup>+</sup>-ATPase. *Science* **334**, 678–683.

STAR★METHODS

KEY RESOURCES TABLE

| REAGENT or RESOURCE                                  | SOURCE                            | IDENTIFIER                    |
|--|-----------------------------------|-------------------------------|
| <b>Antibodies</b>                                    |                                   |                               |
| Rabbit anti-phospho-S6K-T389                         | Cell Signaling Technology         | cat.#9234; RRID: AB_2269803   |
| Rabbit anti-S6K                                      | Cell Signaling Technology         | cat.#2708                     |
| Rabbit anti-phospho-4EBP1-T37/46                     | Cell Signaling Technology         | cat.#2855                     |
| Rabbit anti-4EBP1                                    | Cell Signaling Technology         | cat.#9644; RRID: AB_2097841   |
| Rabbit anti-phospho-4EBP1-S65                        | Cell Signaling Technology         | cat.#9451; RRID: AB_330947    |
| Rabbit anti-phospho-4EBP1-T70                        | Cell Signaling Technology         | cat.#9455; RRID: AB_330949    |
| Rabbit anti-phospho-mTOR-S2448                       | Cell Signaling Technology         | cat.#2971; RRID: AB_330970    |
| Rabbit anti-phospho-mTOR-S2481                       | Cell Signaling Technology         | cat.#2974; RRID: AB_2262884   |
| Rabbit anti-mTOR                                     | Cell Signaling Technology         | cat.#2983; RRID: AB_2105622   |
| Rabbit anti-phospho-Rictor-T1135                     | Cell Signaling Technology         | cat.#3806; RRID: AB_10557237  |
| Rabbit anti-Rictor                                   | Cell Signaling Technology         | cat.#2140; RRID: AB_2179961   |
| Rabbit anti-phospho-ULK1-S757                        | Cell Signaling Technology         | cat.#6888; RRID: AB_10829226  |
| Rabbit anti-phospho-ULK1-S638                        | Cell Signaling Technology         | cat.#14205; RRID: AB_2798424  |
| Rabbit anti-phospho-Grb10-S476                       | Cell Signaling Technology         | cat.#11817; RRID: AB_2797735  |
| Rabbit anti-GADPH                                    | Cell Signaling Technology         | cat.#2118                     |
| Mouse anti-HA  | Santa Cruz Biotechnology          | cat.sc-7392                   |
| Rabbit anti-ULK1                                     | Sigma-aldrich                     | cat.A7481; RRID: AB_1840703   |
| Rabbit anti-ATP6V1G1                                 | Sigma-aldrich                     | cat.#SAB1305279               |
| Mouse anti-actin                                     | Sigma-aldrich                     | cat.A5316                     |
| Rat anti-LAMP2                                       | Abcam                             | cat.ab13524; RRID: AB_2134736 |
| HRP-conjugated goat anti-Mouse IgG                   | Millipore                         | cat.AP124P; RRID: AB_90456    |
| HRP-conjugated goat anti-Rabbit IgG                  | Millipore                         | cat.AP132P; RRID: AB_90264    |
| Alexa Fluor 488 donkey anti-rabbit IgG antibody      | Molecular Probes                  | cat.A21206; RRID: AB_2535792  |
| Alexa Fluor 594 donkey anti-rat IgG antibody         | Molecular Probes                  | cat.A21209; RRID: AB_2535795  |
| <b>Bacterial and Virus Strains</b>                   |                                   |                               |
| <i>Actinomadura</i> sp. XM-4-3                       | This paper                        | N/A                           |
| <b>Chemicals, Peptides, and Recombinant Proteins</b> |                                   |                               |
| Verucopeptin   | This paper                        | <a href="#">Data S1</a>       |
| VE-P   | This paper                        | <a href="#">Data S1</a>       |
| NP   | <a href="#">Li et al., 2013</a>   | N/A                           |
| Eq   | <a href="#">Chen et al., 2017</a> | N/A                           |
| Bafilomycin A1                                       | LcLabs                            | E077512                       |
| Torin2   | MCE                               | HY-13002                      |
| Oxaliplatin  | MCE                               | HY-17371                      |
| Doxorubicin  | MCE                               | HY-15142A                     |
| MG132  | MCE                               | HY-13259                      |
| Carboplatin  | meilunbio                         | MB1297                        |
| 17-AAG   | meilunbio                         | MB1634                        |
| Cisplatin  | meilunbio                         | MB1055                        |
| Taxol  | MCE                               | HY-B0015                      |
| Gemcitabine  | meilunbio                         | MB5386                        |
| Mitomycin C  | meilunbio                         | MB1164                        |

(Continued on next page)

**Continued**

| REAGENT or RESOURCE   | SOURCE  | IDENTIFIER   |
|---|---|--------------|
| vincristine   | MCE   | HY-N0488     |
| FITC-dextran  | Sigma   | cat. FD10S   |
| Lysosome Isolation Kit  | Sigma   | cat. LYSIS01 |
| Concanamycin A  | Sigma   | cat. C9705   |
| LysoSensor Green  | Molecular Probes  | cat. L7535   |
| LysoTracker Red   | Beyotime  | C1046        |
| ERTracker Red   | Beyotime  | C1041-1      |
| Mitotracker Red   | Invitrogen  | M22425       |
| Experimental Models: Cell Lines   |   |              |
| 293T(HEK)   | Conservation Genetics CAS Shanghai Cell Bank                            | GNHu17       |
| A375  | Conservation Genetics CAS Shanghai Cell Bank                            | SCSP- 533    |
| A375-HA-V1G1(WT)  | This paper  | N/A          |
| A375-HA-V1G1(L99S)  | This paper  | N/A          |
| A375-HA-V1G1(C104Y)   | This paper  | N/A          |
| A375-HA-V1G1(L99SC104Y)   | This paper  | N/A          |
| A375-RAG <sup>active</sup>  | This paper  | N/A          |
| U2OS  | Conservation Genetics CAS Shanghai Cell Bank                            | KCB200962YJ  |
| U2OS-HA-V1G1(WT)  | This paper  | N/A          |
| U2OS-HA-V1G1(L99S)  | This paper  | N/A          |
| U2OS-HA-V1G1(C104Y)   | This paper  | N/A          |
| U2OS-HA-V1G1(L99S C104Y)  | This paper  | N/A          |
| U2OS-RAG <sup>active</sup>  | This paper  | N/A          |
| SGC7901/VCR   | Conservation Genetics CAS Shanghai Cell Bank                            | TCHu 46      |
| K562R   | R. Ren's labortary in Shanghai Institute of Hematology, Shanghai, China | N/A          |
| Experimental Models: Organisms  |   |              |
| BALB/c nude mice  | Beijing Vital River Laboratory Animal Technology                        | N/A          |
| Oligonucleotides  |   |              |
| sgRNA targeting sequence: ATP6V1G1(#1):<br>5'-cccctgagactgactagcca-3'     | <a href="http://crispr.mit.edu">http://crispr.mit.edu</a>               | N/A          |
| sgRNA targeting sequence: ATP6V1G1(#2):<br>5'-cccctgagactgactagcca-3'     | <a href="http://crispr.mit.edu">http://crispr.mit.edu</a>               | N/A          |
| shRNA targeting sequence:<br>ATP6V1G1(#1):5'-TGGCTAGTC<br>AGTCTCAGGGGA-3' | This paper  | N/A          |
| shRNA targeting sequence:<br>ATP6V1G1(#2):5'-ACCATCCTC<br>CAGACATACTTC-3' | This paper  | N/A          |
| Recombinant DNA   |   |              |
| pcDNA3.3-HA-V1G1(WT)  | This paper  | N/A          |
| pcDNA3.3-HA-V1G1 L99S   | This paper  | N/A          |
| pcDNA3.3-HA-V1G1 C104Y  | This paper  | N/A          |
| pcDNA3.3-HA-V1G1 L99SC104Y  | This paper  | N/A          |
| pBOBI-HA-V1G1(WT)   | This paper  | N/A          |
| pBOBI-HA-V1G1 L99S  | This paper  | N/A          |
| pBOBI-HA-V1G1 C104Y   | This paper  | N/A          |

(Continued on next page)

**Continued**

| REAGENT or RESOURCE     | SOURCE            | IDENTIFIER  |
|-------------------------|-------------------|---|
| pBOBI-HA-V1G1 L99SC104Y | This paper        | N/A   |
| pBOBI-HA-RagA Q66L      | This paper        | N/A   |
| pBOBI-HA-GST-RagB Q99L  | This paper        | N/A   |
| pBOBI-HA-RagC S75L      | This paper        | N/A   |
| pBOBI-HA-RagD S77L      | This paper        | N/A   |
| Software and Algorithms |                   |   |
|                         | This paper        | N/A   |
| Prism6                  | Graphpad software | <a href="https://www.graphpad.com/">https://www.graphpad.com/</a>   |
| MNova 12.0              | Mestrelab         | <a href="https://mestrelab.com/download_file/mnova-12-0-0/">https://mestrelab.com/download_file/mnova-12-0-0/</a> |

**RESOURCE AVAILABILITY**

**Lead Contact**

Further information and requests for resources and reagents should be directed to and will be fulfilled by the lead contact, Xianming Deng ([xmdeng@xmu.edu.cn](mailto:xmdeng@xmu.edu.cn)).

**Materials Availability**

Plasmids and compounds generated in this study are available upon request to the lead contact.

**Data and Code Availability**

The data supporting the findings of this study are available within the article and its supplementary materials.

**EXPERIMENTAL MODEL AND SUBJECT DETAILS**

**Cell Culture**

MEFs (male mouse origin), HEK293T (female human origin), A375 (female human origin), U2OS (female human origin), SGC7901/VCR (female human origin) cells were cultured in Dulbecco's modified eagle medium (DMEM; Gibco, cat.12800), HL-60 (female human origin) and K562R (female human origin) cells were cultured in Roswell Park Memorial Institute medium (RPMI1640; Gibco, cat. 31800) at 37°C in a humidified incubator containing 5% CO<sub>2</sub>. All media were supplemented with 10% fetal bovine serum (FBS; GEMINI, cat.900-108), 100 µg/mL streptomycin and 100 IU/mL penicillin.

**Mice**

All animal experiments were performed in compliance with the guidelines from the Institutional Animal Care and Use Committee at Experimental Animal Centre in Xiamen University (XMULAC20190032). BALB/c nude mice in half genders (4-6 weeks) were purchased from Beijing Vital River Laboratory Animal Technology Co., Ltd. (Beijing, China). All mice were fed a standard chow diet ad libitum and housed in a Biosafety Level 2 SPF barrier facility at Xiamen university laboratory animal center with standard controlled temperature, humidity, and light-dark cycle (12 h) conditions with no more than 5 mice per cage under the supervision of veterinarians. All experiments were performed on balanced cohorts of male and female mice as our preliminary data did not indicate significant differences in disease progression or response to treatment between males or females. All mice were numbered and experiments were conducted in a blinded fashion. Before all treatments, mice were relocated at random from a housing cage to treatment or control cages.

**METHOD DETAILS**

**Fermentation and Extraction**

Large amount of VE was obtained from the strain *Actinomadura* sp. XM-4-3 in our lab. Strain *Actinomadura* sp. XM-4-3 was isolated from mangrove rhizosphere soil collected at Xiamen, China. The strain was cultured on YMG medium at 28°C for 20 days. 20 liters of fermented agar cakes were diced and extracted with EtOAc–MeOH–AcOH (v/v/v, 80/15/5, 3 × 4 L). After removal of solvents under vacuum, the extract was suspended in EtOAc and washed with water, then the EtOAc fraction was concentrated and resuspended in MeOH and petroleum ether. The MeOH layer was concentrated to afford the defatted extract. Through a series of chromatographic methods including medium-pressure liquid chromatography (MPLC), Sephadex LH-20, HPLC XDB C18 to afford VE.

### Large Panel of Cancer Cells Profiling for VE

Large panel of cancer cell profiling for VE was performed at the Massachusetts General Hospital Cancer Center (Harvard Medical School) as previously described (Garnett et al., 2012). Briefly, Cells were seeded in 384-well microplates in medium supplemented with 5% FBS and penicillin/streptavidin. The optimal cell number for each cell line was determined to ensure that each cell line was in logarithmic phase at the end of the assay. Adherent cell lines were plated 1 day before treatment with a 9-point twofold dilution series of VE using liquid handling robotics, and incubated for 72 h. Cells were then fixed in 4% formaldehyde for 30 min and stained with 1  $\mu$ M of the fluorescent nucleic acid stain Syto60 (Invitrogen) for 1 h. Suspension cell lines were treated with VE immediately following plating, after time line of 72 h, and then stained with 55  $\mu$ g mL<sup>-1</sup> resazurin (Sigma) for 4 h. Quantification of fluorescent signal intensity was performed using a fluorescent plate reader at excitation and emission wavelengths of 630/695nm for Syto60, and 535/595nm for resazurin. This data is included in [Table S1](#).

### Cell Viability Assay

Cells were plated at appropriate density in 96-well plates and allowed to attach overnight. Cells were treated for 48 hours in the presence of increasing concentrations of compounds, and cell viability was then measured using the MTS assay (Promega, cat. G111A). 20  $\mu$ L of MTS reaction solution containing 100  $\mu$ g/mL PES was added to each well. After 1 to 4 h incubation, the absorbance values were detected by spectrophotometer (Varioskan Flash, Thermo, USA) at 490 nm wavelength. IC<sub>50</sub> was calculated based on cell viability dose-response curves by GraphPad Prism6. IC<sub>50</sub> values were averaged over three independent experiments.

### Cytological Profiling

Cytological profiling was performed at the UC Santa Cruz Chemical Screening Center as previously described (Schulze et al., 2013). Briefly, HeLa cells cultured in 384-well plates were treated with test compounds in a range from nanomolar to micromolar concentration or with DMSO alone for 20 hours, after which with fluorescent probes targeting actin (phalloidin), tubulin ( $\alpha$ -tub), total DNA (Hoechst), newly synthesized DNA (EdU), and phosphohistone H3 ( $\alpha$ -pHH3). The plates were imaged using an ImageXpress Micro epifluorescent micro-scope (Molecular Devices) with a 103 Nikon objective lens. Four images were obtained per well for each wavelength in a plate resulting in 4,608 images for the nuclear stain set and 6,144 images for the cytoskeletal stain set. The plates were analyzed using MetaXpress (Molecular Devices). Measurements were taken using built-in morphometry metrics, the multiwavelength cell scoring, transfluor, and micronuclei modules as described. These measurements were converted to feature scores, clustered using the Cluster 3.0 software, and analyzed using Java TreeView.

### Immunoblotting

After treatment, cells were washed and lysed with lysis buffer (50 mM Tris-HCl, 150 mM NaCl, 1% (v/v) Triton X-100, 5% glycerol, 1 mM phenylmethylsulfonyl fluoride, 5  $\mu$ g/mL leupeptin, 1 mM sodium orthovanadate and 50 mM sodium fluoride, pH 7.5). Protein extracts were resolved by SDS-PAGE electrophoresis, blotted with appropriate antibodies and finally detected by WesternBright ECL (advansta, cat. K-12045-D50). Images were performed using a ChemiDoc™ XRS+ System (Bio-rad).

### Immunoprecipitation

Cell lysates were prepared in a lysis buffer (50 mM Tris-HCl, pH 7.4, 150 mM NaCl, 100 mM NaF, 0.5% NP-40, 1 mM phenylmethylsulfonyl fluoride). The lysates were clarified by centrifugation at 13,000 rpm for 30 mins. Then the protein extracts were subjected to immunoprecipitation using specific antibodies in combination with protein G-Sepharose for 3 hours. Precipitated immunocomplexes were washed three times with lysis buffer and then mixed with an equal volume of SDS sample buffer for immunoblotting.

### Immunofluorescence Staining

Cells were seeded on coverslips and fixed with 4% (v/v) PFA for 15 min at room temperature after compound treatment. Then samples were permeabilized with 0.1% Triton X-100 for 5 min. Followed by 5% BSA blocking for 30 min at RT, the primary antibodies (for mTOR, Cell Signaling Technology, cat.#2983 diluted 10  $\mu$ g/ml in PBS; for LAMP2, Abcam, cat.#ab13524, diluted 1:100 in PBS) were incubated with cells overnight at 4°C. After washing 3 times with PBS, the cells were incubated for another 3 h at room temperature with FITC-conjugated Donkey anti-goat IgG (BBI Life Sciences, cat.D110111, diluted 1:100 in PBS) and Alexa-Fluor 594-conjugated anti-mouse secondary antibody (Molecular Probes, cat.11032, diluted 1:100 in PBS), then the samples were washed three times with PBS. All images were collected with a confocal laser scanning microscope Leica TCS SP8.

### Annexin V-FITC/PI Assay

Cell death was quantified using Annexin V-FITC/PI assay according to the manufacturer's protocol (Annexin V-FITC/PI Apoptosis Detection Kit; Vazyme, cat. A 211-02). After treatment, cells were harvested and washed twice with cold PBS buffer and then about 1 x 10<sup>5</sup> cells were resuspended with 100  $\mu$ L binding buffer in 5 mL tube. 5  $\mu$ L Annexin V-FITC and 5  $\mu$ L PI staining solution were added to each tube in the dark and incubated for 10 minutes at room temperature. Then added 400  $\mu$ L binding buffer to each tube before detecting. Data were analyzed by a FC500 flow cytometer (Beckman coulter) and FlowJo and were representative of three independent experiments

### Inducing of VE Resistance in U2OS Cells

To generate VE resistant in U2OS cells, two 10 cm<sup>2</sup> plates of parental U2OS cells at 50% confluence (2 × 10<sup>6</sup> cells/plate) were treated with 50 nM VE for 1 month with media change every 1 to 2 days. The growth state and morphology change of cells were observed every day. Clones that appeared after the selection was then expanded normally at a final concentration of 500 nM VE in 6 well plates. Whole-RNA sequencing of VE resistant U2OS and parental U2OS cells were performed.

### Knock down Experiments

The oligonucleotides were cloned into the lentiviral vector Tet-pLKO-puro (Addgene plasmid 21915). The lentiviruses were generated by transfecting HEK293T cells together with the lentiviral vector and packaging plasmids (pMDL, pVSV-G and pREV). After 48h culturing, the viral supernatants were filtered with a 0.22 μm filter and then were used to transduce A375 and U2OS cells. After drug-selected with puromycin for 1 week, surviving pools were split to 6 well plates and inducing shRNA expression with 1 μg/mL doxycycline. The oligonucleotides sequences for the Tet-pLKO-puro were as follows:

shRNA-ATP6V1G1#1,5'- TGGCTAGTCAGTCTCAGGGGA -3'; shRNA-ATP6V1G1#2,5'- ACCATCCTCCAGACATACTTC-3'; shRNA-Control, 5'- CAACAAGATGAAGAGCACCAA -3'.

### Transient Transfection and Lentivirus Infection

The target of interest was first cloned into the pCDNA3.3 vector for transient transfection or into pBOBI for lentivirus packaging. Total DNA for each plate was adjusted to the same amount. HEK293T cells were transfected with a final concentration of 10 μM PEI and harvested at 48 h after transfection. The lentivirus was generated by transfecting HEK293T cells together with the lentiviral vector and packaging plasmids (pMDL, pVSV-G and pREV) using Lipofectamine 3000 in 6 well plates. After culture for 48 h, the viral supernatants were filtered with a 0.22 μm filter and then were used to infect parental cells for 24 h.

### Chemical Labelling of VE-P and Fluorescence Microscopy

Cells were treated with 500 nM VE-P or DMSO for 1 hour followed by UV(365 nm)-irradiated for 20 min. Lyso-Tracker Red, Mito-Tracker™ Red CMXROS or ER-Tracker Red was added into the culture medium for 40 min incubation. Cells were then fixed with 4% PFA for 15 min, prior to permeabilization (Triton X-100, 0.1% in PBS, 5 min) and washed three times with 1% BSA/PBS. Samples were incubated with the click reaction cocktail (1 μM rhodamine-N<sub>3</sub>, 1 μM TBTA, 10 μM TCEP, and 10 μM CuSO<sub>4</sub>) in the dark at room temperature for 30 min, then washed three times with PBS and counterstained with DAPI (1 μg/mL). Fluorescence images were acquired and processed using a confocal laser scanning microscope Leica TCS SP8.

### Pull-down Assay and LC-MS/MS Analysis

Cellular lysates were supplemented with 200 μL of 5 × HEPES buffer and adjusted to 1 mL with Milli-Q water. A solution of VE-P was added, followed by incubation at 4°C for 2 h. The reaction mixture was then UV (365 nm)-irradiated for 20 min before addition of biotin-N<sub>3</sub> under click conditions (a freshly premixed click chemistry reaction cocktail in PBS contains 0.1 mM biotin-N<sub>3</sub>, 0.1 mM TBTA, 1 mM TCEP, and 1 mM CuSO<sub>4</sub>). Upon acetone precipitation and resolubilization (in PBS with 1% SDS with brief sonication), the resuspended sample was incubated with avidin-agarose beads at 4°C overnight. After centrifugation, the supernatant was removed and the beads were washed with PBS three times, finally subjected to LC-MS/MS analysis or immunoblotting.

For LC-MS/MS analysis, U2OS cell lysates were incubated with either VE-P in duplicate or a negative control probe (NP). After click chemical labeling, the biotinylated protein complexes were then pulled down with streptavidin beads. The beads were boiled and resolved by SDS-PAGE. After staining of gels with Coomassie blue, excised gel segments were subjected to in-gel trypsin digestion and dried. Samples were analyzed on a nanoElute (Bruker) coupled to a timsTOF Pro (Bruker) equipped with a CaptiveSpray source. Peptides were dissolved in 10 μL 0.1% formic acid and were auto-sampled directly onto a homemade C18 column (35 cm × 75 μm i.d., 1.9 μm 100 Å). Samples were then eluted for 60 mins with linear gradients of 3–35% acetonitrile in 0.1% formic acid at a flow rate of 300 nL/min. Mass spectra data were acquired with a timsTOF Pro mass spectrometer (Bruker) operated in PASEF mode. The raw files were analyzed by Peaks Studio X software against uniprot database. More than two thousands of proteins were identified in each group. Among them, 1551 proteins that present in both VE groups but not in NP group were classified as VE-associated proteins for further analysis. We identified 84 lysosomal proteins within VE-associated proteins by gene ontology (GO) cellular component (CC) analysis and then subjected to further GO molecular function (MF) analysis. The top term of MF was proton-transporting ATPase activity, rotational mechanism (GO:0046961) clustering a number of lysosome-specific v-ATPase subunits which were list in [Table S3](#). The complete LC-MS/MS data was provided in [Table S2](#).

### Characterization of Verucopeptin (VE)

**VE**, obtained from strain *Actinomadura* sp. XM-4-3, white amorphous powder; [α]<sub>D</sub><sup>25</sup> -20.0 (c 0.2, MeOH); <sup>1</sup>H NMR (CDCl<sub>3</sub>, 600 MHz): δ 0.79 (d, 3H, J = 6.9 Hz, 33-Me), 0.82 (d, 3H, J = 7.5 Hz, 35-Me), 0.86 (t, 3H, J = 6.8 Hz, H37), 0.88 (d, 3H, J = 6.7 Hz, H18), 0.99 (d, 3H, J = 7.2 Hz, 31-Me), 1.01 (m, 1H, H34), 1.04 (m, 1H, H34), 1.05 (m, 1H, H32), 1.09 (d, 3H, J = 6.7 Hz, H19), 1.13 (m, 1H, H36), 1.23 (m, 1H, H32), 1.24 (m, 1H, H36), 1.39 (m, 1H, H35), 1.42 (s, 3H, 23-Me), 1.47 (m, 1H, H11), 1.52 (m, 1H, H33), 1.61 (m, 1H, H11), 1.67 (s, 3H, 29-Me), 1.77 (m, 1H, H17), 1.84 (m, 1H, H26), 1.87 (m, 2H, H25), 1.89 (m, 1H, H12), 2.04 (m, 1H, H26), 2.22 (m, 1H, H12), 2.58 (m, 1H, H31), 2.68 (m, 1H, H13), 2.93 (s, 3H, 6-NMe), 3.07 (m, 1H, H27), 3.13 (s, 3H, 2-NMe), 3.14 (m, 1H, H13), 3.30 (s, 3H, 27-OMe), 3.47 (d, 1H, J = 17.5 Hz, H2), 3.64 (d, 1H, J = 15.4 Hz, H6), 3.69 (d, 1H, J = 17.0 Hz, H4),

3.91 (d, 1H, J = 15.5 Hz, H8), 4.12 (d, 1H, J = 9.3 Hz, H28), 4.14 (d, 1H, J = 15.4 Hz, H6), 4.66 (d, 1H, J = 17.5 Hz, H2), 4.80 (dd, 1H, J = 2.7, 9.6 Hz, H16), 4.89 (13-NH, 1H), 5.07 (dd, 1H, J = 6.6, 17.0 Hz, H4), 5.19 (d, 1H, J = 9.5 Hz, H30), 5.29 (d, 1H, J = 15.5 Hz, H8), 5.33 (d, 1H, J = 7.1 Hz, H10), 6.12 (dd, 1H, J = 2.6, 9.5 Hz, H15), 7.36 (4-NH, 1H), 9.14 (8-NOH, 1H). (Data S1); <sup>13</sup>C NMR (CDCl<sub>3</sub>, 150 MHz): δ 11.5, 11.5, 18.4, 18.5, 19.0, 19.2, 21.3 C23-Me, 21.4, 21.4, 23.9, 24.0, 27.2, 27.7, 29.6, 30.0, 30.4, 31.6, 34.7 C6-NMe, 36.8 C2-NMe, 42.4 C4, 45.0, 46.1, 46.5 C15, 46.9 C13, 48.5 C10, 51.3 C8, 51.8 C2, 52.4 C6, 56.8 C27-OMe, 75.7 C27, 77.6 C23, 79.9 C28, 80.0 C16, 98.4 C24, 130.0 C29, 131.7 C30, 167.0, 167.2, 170.9, 171.3, 171.8, 176.1 C22, 176.2 (Data S1); HRMS (ESI-TOF) *m/z*: [M+Na]<sup>+</sup> Calcd for C<sub>43</sub>H<sub>73</sub>N<sub>7</sub>O<sub>13</sub>Na 918.5159, found 918.5141 (Data S1).

### Synthesis of VE-P, NP and Eq

Reagents for chemical reactions were purchased from Sigma-Aldrich without purification unless mentioned otherwise. Reactions were monitored by thin layer chromatography (TLC) on glass plates coated with silica gel (200–300 mesh, Qingdao Marine Chemical Plant). Column chromatography was performed with silica gel (200–300 mesh, Qingdao Marine Chemical Plant), reversed-phase RP-18 (40–63 μm, Merck), and Sephadex LH-20 (Amersham Biosciences). Optical rotations were measured on AUTOPOL IV automatic polarimeter (RUDOLPH Inc). Mass spectra for compound characterization were collected by Waters Acuity SQD LC-MS with the mode of electron spray ionization (ESI). High resolution mass spectra were obtained on Thermo Fisher scientific LTQ FTICR-MS. Compounds were purified by Agilent high performance liquid chromatograph (HPLC) with an Agilent Eclipse XDB-C18 column (5 μm, 9.4×250 mm). NMR spectra were measured on a Bruker Ultrashield Plus-600 (600 MHz) and a Bruker AVANCE III (850MHz) instrument using TMS as the internal standard, and chemical shift were report in δ (ppm), multiplicities (s = singlet, d = doublet, t = triplet, q = quartet, p = pentet, m = multiplet, and br = broad), integration and coupling constants (*J* in Hz). <sup>1</sup>H and <sup>13</sup>C chemical shift are relative to the solvent: δ<sub>H</sub> 7.26 and δ<sub>C</sub> 77.0 for CDCl<sub>3</sub>; δ<sub>H</sub> 2.50 and δ<sub>C</sub> 39.5 for DMSO-d<sub>6</sub>.

To the solution of verucopeptin (5 mg, 5.58 μmol) in DMF (0.2 mL) were added DMAP (2.0 mg, 16.7 μmol), EDC·HCl (3.2 mg, 16.7 μmol) and 3-(3-(but-3-yn-1-yl)-3H-diazirin -3-yl)propanoic acid (0.9 mg, 5.58 μmol) and the mixture were stirred at room temperature for 4 hours in the dark, the residue was purified by semi-preparative HPLC in mobile phase (acetonitrile:H<sub>2</sub>O = 85:15) containing 0.02% Trifluoroacetic acid to give compound VE-P (1.0 mg, 17.2%).

**VE-P**, white amorphous powder, <sup>1</sup>H NMR (DMSO-d<sub>6</sub>, 850 MHz): δ 0.77 (d, 3H, overlap), 0.81 (d, 3H, overlap), 0.84 (t, 3H, overlap), 0.88 (d, 3H, overlap), 0.89 (d, 3H, overlap), 0.97 (m, 1H), 1.03 (m, 1H), 1.03 (m, 1H), 0.85–0.90 (d, 6H), 1.11 (m, 1H), 1.15 (m, 1H), 1.24 (m, 1H), 1.39 (m, 1H), 1.23 (s, 3H), 1.48 (m, 1H), 1.52 (m, 1H), 1.65 (m, 1H), 1.66 (m, 1H, H-P7), 1.57 (s, 3H), 1.77 (m, 1H), 1.84 (m, 1H), 1.86 (m, 2H), 1.74 (m, 1H), 1.95 (m, 1H), 1.94 (m, 1H), 2.28 (m, 1H), 2.28 (m, 1H, H-P7), 2.72 (m, 1H, H13), 2.99 (s, 3H, 6-NMe), 2.83 (m, 1H, H-P1), 2.97 (m, 1H, H27), 3.09 (s, 3H, 2-NMe), 3.00 (m, 1H, H13), 3.16 (s, 3H, 27-OMe), 3.93 (d, 1H, J = 17.8 Hz, H2), 4.60 (d, 1H, overlap H6), 3.84 (d, 1H, overlap H4), 3.80 (d, 1H, overlap H8), 3.87 (d, 1H, overlap H28), 4.92 (d, 1H, overlap H6), 4.19 (d, 1H, J = 17.8 Hz, H2), 4.89 (dd, 1H, J = 2.7, 9.6 Hz, H16), 4.10 (dd, 1H, overlap H4), 5.00 (d, 1H, J = 9.0 Hz, H30), 4.11 (d, 1H, overlap H8), 5.50 (d, 1H, H10), 5.87 (dd, 1H, J = 2.8, 9.0 Hz, H15), 7.48 (4-NH, 1H). (Data S1); <sup>13</sup>C NMR (DMSO-d<sub>6</sub>, 212 MHz): δ 11.8, 13.0, 15.7, 19.4, 19.5, 19.6, 19.7, 20.2, 20.9, 21.9, 22.0, 22., 22.3, 24.4, 26.0 C-P7, 27.5, 28.2, 29.3, 30.1, 31.4, 31.6, 32.2, 36.2 C6-NMe, 36.9 C2-NMe, 41.0 C4, 45.0, 46.1, 46.7 C15, 46.2 C13, 49.5 C10, 50.9 C8, 51.4 C2, 52.4 C6, 56.5 C27-OMe, 72.3 C-P1, 75.5 C27, 76.9 C23, 79.8 C28, 78.2 C16, 83.6 C-P2, 207.7 C24, 133.0 C29, 135.5 C30, 166.7, 168.6, 168.6, 169.1 C-P8, 170.0, 170.6, 171.0, 176.7 C22; HRMS (ESI-TOF) *m/z*: [M+NH<sub>4</sub>]<sup>+</sup> Calcd for C<sub>51</sub>H<sub>85</sub>N<sub>10</sub>O<sub>14</sub> 1061.6241, found 1061.6276 (Data S1).

Negative probe (**NP**) was synthesized as described (Li et al., 2013). Briefly, To the solution of aniline (50 mg, 0.54 mmol) in DMF (3 mL) were added DMAP (80 mg, 0.67 mmol), EDC·HCl (100 mg, 0.55 mmol) and 3-(3-(but-3-yn-1-yl)-3H-diazirin -3-yl)propanoic acid (80 mg, 0.5 mmol) and the mixture was stirred at room temperature for 24 hours in the dark, the residue was purified by silica gel chromatography (1–5% MeOH gradient in CH<sub>2</sub>Cl<sub>2</sub>) to give compound **NP** (90 mg, 80%).

**NP**, <sup>1</sup>H NMR (600 MHz, CDCl<sub>3</sub>) δ 7.51 (d, J = 7.9 Hz, 2H), 7.34 (t, J = 7.9 Hz, 2H), 7.24 (s, 1H), 7.14 (t, J = 7.4 Hz, 1H), 2.17–2.11 (m, 2H), 2.06 (td, J = 7.4, 2.6 Hz, 2H), 2.01 (t, J = 2.7 Hz, 1H), 1.96 (t, J = 7.6 Hz, 2H), 1.70 (t, J = 7.4 Hz, 2H); MS (ESI) *m/z*: 242 [C<sub>14</sub>H<sub>15</sub>N<sub>3</sub>O + H]<sup>+</sup>

Electrophilic quinazolines (**Eq**) was synthesized as described (Chen et al., 2017). Briefly, to a solution of 4-chloro-7-nitroquinazoline (60 mg, 0.29 mmol) in isopropanol (2 mL) was added 3-ethynylaniline (35 mg, 0.30 mmol). The reaction mixture was stirred at room temperature for 10 h and then cooled in an ice bath. The precipitate was collected through filtration and dried over vacuo to afford *N*-(3-ethynylphenyl)-7-nitroquinazolin-4-amine (80 mg). The residues were further suspended in methanol (2 mL), and NH<sub>4</sub>Cl (98 mg, 1.8 mmol) and Zn powder (100 mg, 1.5 mmol) were added. The reaction mixture was sonicated for 5 min and stirred at RT for 24 h. The reaction mixture was filtered to remove the residual zinc powder, which was then concentrated in vacuo. The residues were diluted with EtOAc and washed with saturated NaHCO<sub>3</sub> solution. The basic layer was further extracted with EtOAc twice. The combined organic phases were washed with brine, and concentrated under reduced pressure to provide *N*<sup>4</sup>-(3-ethynylphenyl)quinazoline-4,7-diamine (50 mg, 70%).

To a solution of *N*<sup>4</sup>-(3-ethynylphenyl)quinazoline-4,7-diamine (50 mg, 0.19 mmol) in THF/CH<sub>2</sub>Cl<sub>2</sub> (5:1, 3.0 mL) DIPEA (100 μL, 0.58 mmol) was added and stirred for 10 min. Chloroacetylchloride (23 μL, 0.29 mmol) was added to the reaction mixture and stirred for another 1 h, the mixture was diluted with EtOAc, and washed with saturated NaHCO<sub>3</sub> solution. The aqueous phase was extracted with EtOAc twice and the combined organic phases were concentrated in vacuo, and purified by silica gel chromatography (1–5% MeOH gradient in CH<sub>2</sub>Cl<sub>2</sub>) to afford Eq (13 mg, 20%).

**Eq.** <sup>1</sup>H NMR (600 MHz, DMSO-d<sub>6</sub>) δ 10.76 (s, 1H), 9.83 (s, 1H), 8.61 (s, 1H), 8.51 (d, J = 9.0 Hz, 1H), 8.15 (d, J = 2.2 Hz, 1H), 8.06 (t, J = 1.9 Hz, 1H), 7.90 (dd, J = 7.6, 2.1 Hz, 1H), 7.75 (dd, J = 9.0, 2.2 Hz, 1H), 7.41 (t, J = 7.9 Hz, 1H), 7.23 (dt, J = 7.6, 1.3 Hz, 1H), 4.36 (s, 2H), 4.21 (s, 1H). MS(ESI) *m/z*: 336 [C<sub>18</sub>H<sub>13</sub>ClN<sub>4</sub>O + H]<sup>+</sup>

### Isolation of Light Organelles

Light organelles were isolated as described previously (Steinberg et al., 2010; Zoncu et al., 2011). Briefly, cells were scraped and spun down at 200 *g* at room temperature, and then resuspended in 750 μL per 15-cm dish of fractionation buffer (140 mM KCl, 1 mM EGTA, 5 mM MgCl<sub>2</sub>, 50 mM sucrose, 20 mM HEPES, pH 7.4, supplemented with 2.5 mM ATP, amino acids (Gibco, cat. 11130-077) and protease inhibitor cocktail) at room temperature, and were mechanically broken by spraying 6 times through a 22G needle, yielding post-nuclear supernatants (PNS) after spinning at 2,000 *g* for 5 min. The PNS was then spun at max speed for 15 min in a tabletop centrifuge. The pellets are light organelles and supernatants are the cytosol.

### Purification of Lysosomes

Lysosomes were purified by Lysosome Isolation Kit according to the manufacturer's instructions, with minor modifications. Briefly, MEFs from sixty 10-cm dishes (60-80% confluence) were collected by directly scrapping at room temperature, followed by centrifugation for 5 min at 500*g* at 37°C. Cells were resuspend in 7 mL of 1 × Extraction Buffer containing protease inhibitor cocktail at room temperature, and were dounced in a 7-mL Dounce homogeniser (Sigma, cat. P0610) for 120 strokes on ice followed by centrifuging for 10 min at 1,000 *g*, 4°C, yielding post-nuclear supernatants (PNS). The PNS were then centrifuged for 20 min at 20,000*g* and the pellet was suspended by 1 × Extraction Buffer by gentle pipetting, generating Crude Lysosomal Fraction (CLF). The volume of CLF was adjusted to 2.4 mL and then equally divided into six 1.5 mL Eppendorf tubes (400 μL per tube). 253 μL of OptiPrep and 137 μL of 1 × OptiPrep Dilution Buffer were added to each CLF, and mixed by gentle pipetting. The mixture is defined as the Diluted OptiPrep Fraction (DOF). Each DOF (0.8 mL) was loaded to an 11 × 60 mm centrifuge tube at the top of 27% (0.4 mL) and 22.5% (0.5 mL) OptiPrep solution cushions, and then overlaid with 16% (1 mL), 12% (0.9 mL) and 8% (0.3 mL) OptiPrep solutions. The tube was then centrifuged on a SW60 Ti rotor (Beckman) at 150,000*g* for 4 h at 4°C, and the fraction at the top of 12% OptiPrep solution was collected as the crude lysosome fraction. The fraction was diluted with two volumes of PBS, followed by centrifugation at 20,000 *g* for 20 min. The supernatant was then aspirated, and the sediment was the lysosome fraction.

### Measurement of V-ATPase Activity In Vitro

For each assay, lysosomes purified from two 10-cm dishes of MEFs were used. ATP hydrolysis activity was measured using a coupled spectrophotometric method as described previously (Shao and Forgac, 2004) with some modifications. Briefly, lysosomes were suspended in ATPase assay buffer (50 mM NaCl, 30 mM KCl, 20 mM HEPES-NaOH, pH 7.0, 10% glycerol, 1 mM MgCl<sub>2</sub>, 1.5 mM phosphoenolpyruvate, 0.35 mM NADH, 20 U/mL pyruvate kinase, and 10 U/mL lactate dehydrogenase) with 5 μM ConA (for calculating the v-ATPase-specific ATP hydrolysis activity) or DMSO, and warmed at 37°C for 10 min. The assay was initiated by the addition of 5 mM ATP, and the OD<sub>341</sub> was continuously recorded by a SpectraMax M5 microplate reader.

ATP-dependent proton transport activity was measured by the initial rate of ATP-dependent fluorescent quenching of FITC-dextran, as described previously (Lieberman et al., 2014; Trombetta et al., 2003). Briefly, lysosomes were loaded with FITC-dextran by incubating cells in DMEM supplemented with 2 mg/mL FITC-dextran (final concentration) on ice for 5 min, then transferred to a 37°C incubator for 30 min. Cells were washed with DMEM for three times and incubated with DMEM for another 30 min at 37°C to allow transport of FITC-dextran to lysosomes. Cells were collected and lysosomes were purified as described above. The lysosomes were resuspended in assay buffer (125 mM KCl, 1 mM EDTA, 20 mM HEPES, pH 7.5, with KOH) and were balanced on ice for 1 hr, then mixed with 5 μM ConA (for calculating the v-ATPase-specific proton transport activity) or DMSO, then warmed at 37°C for 10 min. Fluorescence of FITC was recorded with excitation at 490 nm and emission at 520 nm using a SpectraMax M5 microplate reader. The initial slope of fluorescence quenching was measured after addition of 5 mM Mg-ATP (final concentration). Data is representative of three independent experiments.

### In Vivo Assay

BALB/c nude mice (4-6 weeks) were purchased from Beijing Vital River Laboratory Animal Technology Co., Ltd. (Beijing, China). Xenografts were initiated by subcutaneous injection of SGC7901/VCR cells (3 × 10<sup>7</sup> cells per mouse). When tumor size reached to approximately 100 mm<sup>3</sup>, mice were randomized to two groups. The mice were i.v. injected with VE by 1 mg kg<sup>-1</sup> twice every day. Mice in the vehicle group received saline (containing 1% DMSO) only. Mice were then examined for tumor growth and body weight changes using a slide caliper (Mitutoyo), and their volumes were calculated using the following formula: a<sup>2</sup> × b × 0.5, where a refers to the smaller diameter and b is the diameter perpendicular to a. At 6 hours of post-final dose, mice were euthanized and tumors were separated and subjected to further analysis. All procedures were performed in compliance with the guidelines from the Institutional Animal Care and Use Committee at Experimental Animal Centre in Xiamen University.

### Hematoxylin and Eosin Staining

Tumor tissues were fixed in 4% paraformaldehyde and embedded in paraffin. Then, 4 μm thick slices were stained with haematoxylin and eosin, then examined by light microscopy (Leica DM4 M).

#### QUANTIFICATION AND STATISTICAL ANALYSIS

The statistical analysis of the difference between two groups was done using the two-tailed Student's *t*-test and multiple groups comparisons were determined using one-way or two-way ANOVA using GraphPad Prism 6 and  $p < 0.05$  was considered statistically significant. Statistical significance is shown as \*  $p < 0.05$ , \*\*  $p < 0.01$ , \*\*\*  $p < 0.001$ .